

**APPLIED PHYSICS REVIEWS**

**Constructal theory of generation of configuration in nature and engineering**

Adrian Bejan<sup>a)</sup>

*Department of Mechanical Engineering and Materials Science, Duke University, Durham, North Carolina 27708-0300*

Sylvie Lorente

*Laboratory for Materials and Durability of Constructions, National Institute of Applied Sciences (INSA), 135 Avenue de Rangueil, Toulouse 31077, France*

(Received 26 April 2006; accepted 19 June 2006; published online 29 August 2006)

Constructal theory is the view that the generation of flow configuration is a physics phenomenon that can be based on a physics principle (the constructal law): “For a finite-size flow system to persist in time (to survive) its configuration must evolve in such a way that it provides an easier access to the currents that flow through it” [A. Bejan, *Advanced Engineering Thermodynamics*, 2nd ed. (Wiley, New York, 1997); *Int. J. Heat Mass Transfer*, **40**, 799 (1997)]. This principle predicts natural configuration across the board: river basins, turbulence, animal design (allometry, vascularization, locomotion), cracks in solids, dendritic solidification, Earth climate, droplet impact configuration, etc. The same principle yields new designs for electronics, fuel cells, and tree networks for transport of people, goods, and information. This review describes a paradigm that is universally applicable in natural sciences, engineering and social sciences. © 2006 American Institute of Physics. [DOI: 10.1063/1.2221896]

**TABLE OF CONTENTS**

I. THE CONSTRUCTAL LAW AND THERMODYNAMICS. . . . .	1	C. Survival by increasing svelteness (compactness). . . . .	22
II. INANIMATE FLOW CONFIGURATIONS. . . . .	2	D. Survival by increasing flow territory. . . . .	23
A. Duct cross sections. . . . .	3	E. Freedom to morph is good for performance..	23
B. Open channel cross sections. . . . .	3	VI. CONCLUSION. . . . .	23
C. Tree-shaped fluid flow river basins. . . . .	4		
D. Turbulent flow structure. . . . .	7	<b>I. THE CONSTRUCTAL LAW AND THERMODYNAMICS</b>	
E. Coalescence of flowing solid packets. . . . .	9	Why is geometry (shape, structure, similarity) a characteristic of natural flow systems? What is the basis for the hierarchy, time evolution, complexity, and rhythm of natural structures? Is there a single physics principle from which form and rhythm can be <i>deduced</i> , without any use of empiricism?	
F. Cracks. . . . .	9	There is such a principle, and it is a summary of common observations that if a flow system is endowed with sufficient freedom to change its configuration, then the system exhibits configurations that provide progressively better access routes for the currents that flow. Observations of this kind come in the billions, and they mean one thing: a time arrow is associated with the sequence of flow configurations that constitutes the <i>existence</i> of the system. In this movie, existing drawings are replaced by easier flowing drawings.	
G. Dendritic crystals. . . . .	9	This principle was formulated in 1996 as the <i>constructal law</i> of the generation of flow configuration. <sup>1-5</sup> “For a flow system to persist in time (to survive) it must evolve in such a way that it provides easier and easier access to the currents that flow through it.” This law is the basis for the constructal	
H. Global circulation and climate. . . . .	10		
III. ANIMATE FLOW CONFIGURATIONS. . . . .	11		
A. Body heat loss versus body size. . . . .	11		
B. Breathing and heartbeating. . . . .	13		
C. Flying. . . . .	13		
D. Running. . . . .	15		
E. Swimming. . . . .	15		
F. Organ size. . . . .	16		
IV. ENGINEERED FLOW CONFIGURATIONS. . . . .	16		
A. Flow spacings. . . . .	16		
B. Trees for heat conduction. . . . .	18		
C. Trees for fluid flow. . . . .	19		
D. Multiobjective flow architectures. . . . .	20		
V. THERMODYNAMICS OF NONEQUILIBRIUM SYSTEMS WITH CONFIGURATION. . . . .	21		
A. Properties. . . . .	21		
B. Survival by increasing performance. . . . .	22		

<sup>a)</sup>Electronic mail: dalford@duke.edu

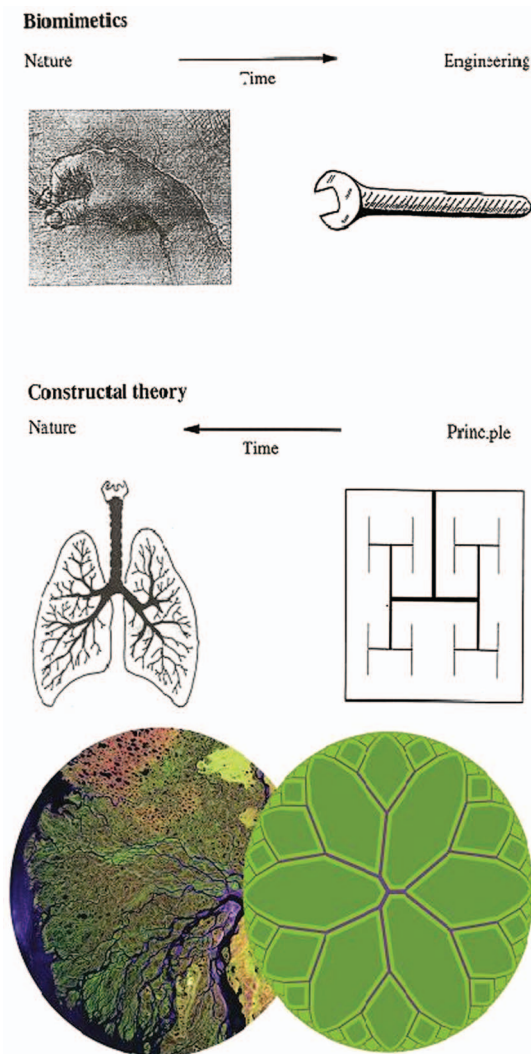


FIG. 1. (Color) Constructal theory proceeds in time against empiricism or copying from nature (Ref. 6). Bottom: the Lena delta and dendritic architecture derived from the constructal law.

theory of the generation of flow configuration in nature<sup>1,6</sup> (Fig. 1). Today this entire body of work represents a new extension of thermodynamics: the thermodynamics of non-equilibrium systems with configuration.<sup>7-12</sup>

To see why the constructal law is a law of thermodynamics (physics), we ask why the constructal law is different than (i.e., distinct from or complementary to) the other laws of thermodynamics. Think of an isolated thermodynamic system that is initially in a state of internal nonuniformity (e.g., regions of higher and lower pressures or temperatures, separated by internal partitions that suddenly break). The first law and the second law account for observations that describe a tendency in time, a time arrow: if enough time passes, the isolated system settles into a state of equilibrium (no internal flows, maximum entropy at constant energy). The first law and second law speak of a black box. They say nothing about the configurations (the drawings) of the things that flow.

Classical thermodynamics is not concerned with the configurations of its nonequilibrium (flow) systems. It should be. After all, Sadi Carnot's memoir is about the improvement

(evolution) of machine configurations in time. This intuition was shared by many who pursued the optimization of thermodynamic performance on an *ad hoc* basis in separate fields (engineering, biology, geophysics, and economics), without recognizing the universality of the configuration-generation *phenomenon* that was put on display by the optimization of thermodynamic performance. The generation of flow configuration is a natural phenomenon, and it belongs in thermodynamics.

This tendency, this time sequence of drawings that the flow system exhibits as it evolves, is the phenomenon covered by the constructal law. Not the drawings *per se*, but the time direction in which they morph if given freedom. No configuration in nature is "predetermined" or "destined" to be or to become a particular image. The actual evolution or lack of evolution (rigidity) of the drawing depends on many factors, which are mostly random, as we will see in Fig. 7.

The same can be said about the second law. No isolated system in nature is predetermined or destined to end up in a state of uniform intensive properties so that all future flows are ruled out. One cannot count on the removal of all the internal constraints.

The second law does proclaim the existence of the concept of equilibrium in an isolated system, at sufficiently long times when all internal constraints have been removed. Likewise, the constructal law proclaims the existence of the concept of equilibrium flow architecture, when all possibilities of increasing morphing freedom have been exhausted.<sup>7,8,13</sup>

Constructal theory is now a fast growing field with contributions from many sources, and with leads in many directions. This body of work has two main parts. The first is the use of the constructal law to predict and explain the occurrence of *natural* flow configurations, inanimate and animate (Secs. II and III). The second part is the application of the constructal law as a physics principle in *engineering*. This activity of *design as science*<sup>14</sup> is reviewed in Secs. IV and V.

Because constructal theory proclaims the oneness of natural and engineered flow configuration generation phenomena, it is important to keep Fig. 1 in mind. Nature and engineering can be contemplated together in two ways, empirically and theoretically. In empiricism, the observing and copying from nature come first, and this serves as basis for modeling, description, and bioinspired engineering. In constructal theory the thought process goes against the time arrow of empiricism: first, the constructal law is invoked, and from this thought the flow architecture is deduced. Only later is the theoretical configuration compared with a natural configuration, and the agreement between the two validates the constructal law.

## II. INANIMATE FLOW CONFIGURATIONS

Classes of inanimate flow configurations that have been treated in detail are the shapes of duct cross sections, the shapes of river cross sections, internal spacings, turbulent flow structures, tree-shaped architectures, dendritic solidification (snowflakes), Bénard convection, and global circulation and climate. In this section we review some of the main features and theoretical conclusions.

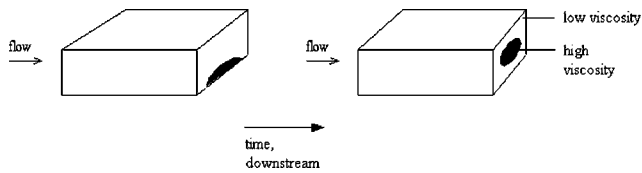


FIG. 2. The evolution of the cross-sectional configuration of a stream composed of two liquids, low viscosity, and high viscosity. In time, the low viscosity liquid coats all the walls, and the high viscosity liquid migrates toward the center. This tendency of “self-lubrication” is the action of the constructal law of the generation of flow configuration in geophysics (e.g., volcanic discharges, drawn after Ref. 16) and in many biological systems.

### A. Duct cross sections

Blood vessels and pulmonary airways have round cross sections. Subterranean rivers, volcanic discharges, earthworms, and ants carve galleries that have round cross sections. These many phenomena of flow configuration generation have been reasoned<sup>1</sup> by invoking the constructal law for the individual duct, or for the larger flow system that incorporates the duct. If the duct has a finite size (fixed cross-sectional area  $A$ ) and the freedom to change its cross-sectional shape, then, in time, the shape will evolve such that the stream that flows through the duct flows with less resistance. If the larger system is isolated and consists of the duct and the two pressure reservoirs connected to the ends of the duct, then the duct architecture will evolve such that the entire system reaches equilibrium (no flow, uniform pressure) the fastest.

The duct cross section evolves in time toward the round shape. This evolution cannot be witnessed in blood vessels and bronchial passages because our observation time scale (lifetime) is too short in comparison with the time scale of the evolution of a living system. The morphing of a round gallery can be observed during erosion processes in soil, following a sudden rainfall. It can be observed in the evolution of a volcanic lava conduit, where lava with lower viscosity coats the wall of the conduit, and lava with higher viscosity positions itself near the central part of the cross section.<sup>15,16</sup>

To have it the other way—high viscosity on the periphery and low viscosity in the center—would be a violation of the constructal law. All phenomena of *self-lubrication* are in accord with the constructal law.

Additional support for the constructal law is provided by laboratory simulations of lava flow with high-viscosity intrusions (Fig. 2). Initially, the intrusion has a flat cross section, and is positioned near the wall of the conduit. In time, i.e., downstream, the intrusion not only migrates toward the center of the cross section but also develops a round cross section of its own. This tendency matches what is universally observed when a jet (laminar or turbulent) is injected into a fluid reservoir.<sup>17,18</sup> If the jet has a flat cross section, then further downstream it develops into one or more thicker jets with round cross sections. The opposite trend is not observed: a round jet does not evolve into a flat jet.

The superiority of the round shape relative to other shapes is an important aspect the generalization of which has become a new addition to the thermodynamics of nonequilibrium systems: the thermodynamics of systems with configuration<sup>7,8,13</sup> (Sec. V). For example, if the duct is

TABLE I. The laminar flow resistances of ducts with regular polygonal cross sections with  $n$  sides (Ref. 1).

$n$	Po	$p/A^{1/2}$	$p^2\text{Po}/A$
3	13.33	4.559	277.1
4	14.23	4	227.6
6	15.054	3.722	208.6
8	15.412	3.641	204.3
$\infty$	16	$2\pi^{1/2}$	201.1

straight and the perimeter of the fixed- $A$  cross section is  $p$  (variable), then the pressure drop ( $\Delta P$ ) per unit length ( $\Delta L$ ) is  $\Delta P/\Delta L = (2f/D_h) \rho V^2$ , the hydraulic diameter is  $D_h = 4A/p$ ,  $V$  is the mean fluid velocity ( $\dot{m}/\rho A$ , fixed), and  $f$  is the friction factor. If the flow regime is laminar and fully developed, then  $f = \text{Po}/\text{Re}$ , where  $\text{Re} = D_h V/\nu$  and  $\text{Po}$  is a factor (called Poiseuille constant) that depends solely on the shape of the cross section. The duct flow resistance is

$$\frac{\Delta P/\Delta L}{\dot{m}} = \frac{\nu}{8A^2} \left( \text{Po} \frac{p^2}{A} \right), \quad (1)$$

where the group in parentheses depends only on the shape of the cross section. This group governs the morphing direction. Table I shows the values of the group ( $\text{Po} p^2/A$ ) for several regular polygonal cross sections. Even though the round shape is the best, the nearly round shapes perform almost as well. The change in  $p^2 \text{Po}/A$  from the hexagon to the circle is only 3.7%. Yet the hexagonal ducts have the great advantage that they can be packed in parallel into bundles, to fill a volume. Square ducts also have this packing advantage, and their flow resistance is only 9.1% greater than that of hexagonal ducts.

Even if the duct cross section is imperfect—that is, with features such as sharp corners, which concentrate fluid friction—its performance is already as good as it can be. Diversity (several near-optimal shapes) goes with the constructal law, not against it. Furthermore, the best performance of all the possible cross sections can be predicted quite accurately when the global constraints ( $A, \dot{m}$ ) are specified.

### B. Open channel cross sections

The conclusions reached above also hold for turbulent flow through a duct, in which the global flow resistance is more closely proportional to  $p^2/A$ , not  $\text{Po} p^2/A$ . This is relevant to understanding why there is proportionality between width ( $W$ ) and maximum depth ( $d$ ) in rivers of all sizes.<sup>19,20</sup> Because of the high Reynolds number and the roughness of the river bed, the skin friction coefficient  $C_f$  is essentially constant. The longitudinal shear stress along the river bottom is fixed ( $\tau = \frac{1}{2} C_f \rho V^2$ ) because  $V = \dot{m}/\rho A$  and the mass flow rate ( $\dot{m}$ ) and the river cross-sectional area ( $A$ ) are fixed. The total force per unit of channel length is  $p\tau$ , where  $p$  is the wetted (bottom) perimeter of the cross section. This means that the constructal law calls for cross-sectional shapes that have smaller  $p$  values.

For example, if the cross section is a rectangle of width  $W$  and depth  $d$ , then  $p = W + 2d$ , and  $A = Wd$ . The minimiza-

TABLE II. Optimized cross-sectional shapes of open channels (Ref. 1).

Cross section	$(W/d)_{\text{opt}}$	$p_{\text{min}}/A^{1/2}$
Rectangle	2	2.828
Triangle	2	2.828
Parabola	2.056	2.561
Semicircle	2	2.507

tion of  $p$  subject to  $A=\text{constant}$  yields  $(W/d)_{\text{opt}}=2$  and the  $p_{\text{min}}/A$  value shown in Table II. Other types of cross sections can be optimized, and the resulting shape and performance are almost the same as for the rectangular case. The semicircular shape is the best, but it is not best by much. Once again, diversity of configurations on the podium of high performance is demanded by the constructal law. What is indeed random, because of local geological conditions (e.g., flat versus curved river bottoms), coexists with pattern: the optimized aspect ratio and the minimized flow resistance  $p_{\text{min}}/A^{1/2}$ .

The two most extreme cases of Table II are separated by only 12% in flow resistance. This high level of agreement with regard to performance is very important. It accounts for the significant scatter in the data on river bottom profiles, if global performance is what matters, not local shape. Again, this is in agreement with the new work on drainage basins (Sec. II C), where the computer-optimized (randomly generated) network looks like the many, never identical networks seen in the field. There is uncertainty in reproducing the many shapes that we see in nature, but this is not the issue. There is no uncertainty in anticipating global characteristics such as performance and geometric scaling laws (e.g.,  $W/d$ ) and allometric scaling laws (Sec. III).

The river banks of the optimal shape (the half circle) extend vertically downward into the water and are likely to crumble under the influence of erosion (drag on particles) and gravity. This will decrease the slopes of the river bed near the free surface and, depending on the bed material, it will increase the slenderness ratio  $W/d$ .

### C. Tree-shaped fluid flow river basins

River basins and deltas, such as the lungs and vascularized tissues of animal design, are dendritic flow structures. The observed similarities between geophysical trees and biological trees have served as basis for modeling and description. In constructal theory tree-shaped flows are not models but solutions to fundamental access-maximization problems: volume point, area point, and line point. Important is the geometric notion that the “volume,” the “area,” and the “line” represent *infinities* of points. The theoretical discovery of trees<sup>1-5</sup> in constructal theory stems from the decision to connect one point (source or sink) with the infinity of points (volume, area, and line).

The two modes of flowing with imperfection (with flow resistance) must be *balanced* so that together they contribute minimum imperfection to the global flow architecture. The flow architecture is the graphical expression of the balance between links and their interstices. The deduced architecture

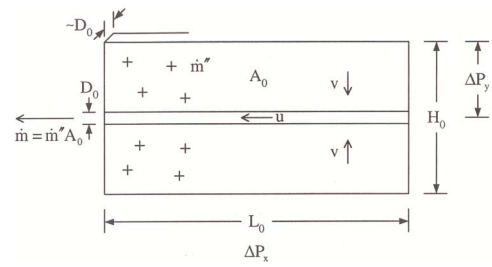


FIG. 3. Elemental area of a river basin viewed from above: seepage with high resistivity (Darcy flow) proceeds vertically, and channel flow with low resistivity proceeds horizontally. Rain falls uniformly over the rectangular area  $A_0=H_0L_0$ . The flow from the area to the point (sink) encounters minimum global resistance when the external shape  $H_0/L_0$  is optimized. The generation of geometry is the mechanism by which the area-point flow system assures its persistence in time, its survival.

(tree, duct shape, spacing, etc.) represents *optimal distribution of imperfection*.

The discovery of constructal tree-shaped flow architectures began with three approaches, two of which are reviewed in this section. The first was an analytical short cut<sup>2,3,5</sup> based on several simplifying assumptions: 90° angles between stem and tributaries, a construction sequence in which smaller optimized constructs are retained, constant-thickness branches, etc. The same problem was treated numerically<sup>21</sup> by abandoning most of the simplifying assumptions (e.g., the construction sequence) used in the first papers. The third approach was fully numerical<sup>22</sup> in an area-point flow domain with random low-resistivity blocks embedded in a high-resistivity background, by using the language of Darcy flow (permeability, instead of thermal conductivity and resistivity). Along the way, these approaches produced better performance and “more natural looking” trees as a progression in time; that is as the problem formulation endowed the flow structure with more freedom to morph.

The first approach is illustrated in Fig. 3. The “elemental area” of a river basin ( $A_0=H_0L_0$ ) is the area allocated to the smallest rivulet (length  $L_0$ , width  $D_0$ , depth scale  $D_0$ , cf. Sec. II B). Rain falls uniformly on  $A_0$  with the mass flow rate  $\dot{m}^*$  [kg s<sup>-1</sup> m<sup>-2</sup>]. Constructal theory predicts an optimal allocation of area to each channel: there is an optimal elemental shape  $H_0/L_0$  such that the total flow rate ( $\dot{m}^*A_0$ ) collected on  $A_0$  escapes with least global flow resistance from  $A_0$  through one port on its periphery. If the water seepage through the wet banks (perpendicular to the rivulet) is in the Darcy flow regime, then the pressure (or elevation) difference that drives the seepage velocity  $v$  is of order  $\Delta P_y \sim v\mu H_0/K$ , where  $K$  is the permeability of the porous medium. If the rivulet flow is in the Poiseuille regime, then the pressure (or elevation) drop along the  $L_0$  rivulet is of order  $\Delta P_x \sim \mu L_0/D_0^2$ . These equations can be combined to conclude that the overall pressure difference that drives the area-point flow is

$$\Delta P_x + \Delta P_y \sim \dot{m}^* v \left( \frac{L_0}{D_0^2} + \frac{H_0}{KL_0 D_0} \right). \quad (2)$$

This global measure of flow imperfection can be minimized with respect to the shape of the area element. The optimal elemental shape is

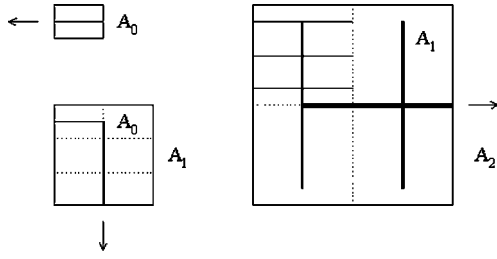


FIG. 4. Constructal sequence of assembly and optimization, from the optimized elemental area ( $A_0$ , Fig. 3) to progressively larger area-point flows (Ref. 23).

$$\left(\frac{L_0}{H_0}\right)_{\text{opt}} \sim \left(\phi_0 \frac{A_0}{K}\right)^{1/3}, \quad (3)$$

where  $\phi_0$  is the area fraction occupied by the rivulet on the flow map,  $\phi_0 = D_0 L_0 / H_0 L_0 \ll 1$ . When the area element has optimal shape,  $\Delta P_y$  is of the same order as  $\Delta P_x$ . This is a frequent occurrence in the maximization of area-point flow access: the optimal partitioning of the driving force between the two flow mechanisms is synonymous with the optimization of flow geometry.<sup>12</sup>

The optimized area element becomes a building block with which larger rain plains can be covered. The elements are assembled and connected into progressively larger area constructs, in a sequence of “assembly+optimization” at every step. During this sequence, the river channels form a tree architecture in which every geometric detail is deduced, not assumed. The construction sequence is illustrated in Fig. 4. Better and more realistic tree architectures are obtained by relaxing the assumption of 90° angles, and optimizing every angle.<sup>21</sup>

For river basins with turbulent flow with constant skin friction coefficient, the constructal sequence shows that the best rule of assembly is quadrupling<sup>23</sup> (note  $A_2 = 4A_1$  in Fig. 4). Constructal river basins are area constructs that grow by roughly a factor of 4 at each new level of assembly. This conclusion coincides with what Ref. 21 showed for area-point conduction with trees of high-conductivity inserts (Sec. IV B). If we neglect the smallest area element where there is a balance between slow flow (seepage through wet ground on the hill slope) and fast flow (the smallest rivulet), then we

can use the quadrupling rule to predict the morphological features of increasingly complex river basins. Table III shows the start of the construction,<sup>23</sup> where  $i$  is the order of the construct,  $A_0$  is the smallest square construct (the equivalent of  $A_1$  in Fig. 4),  $N_i$  is the number of streams of all sizes present on  $A_i$ ,  $L_{Ti}$  is the total length of all the streams present on  $A_i$ ,  $R_{Li}$  is the ratio of the length of the largest stream on  $A_i$  divided by the length of the largest stream on  $A_{i-1}$ ,  $R_{Bi}$  is the number of the largest streams of  $A_{i-1}$  divided by the number of the largest streams of  $A_i$ ,  $D_{oi}$  is called drainage density and is equal to  $L_{Ti}/A_i$ ,  $F_{si}$  is the stream frequency ( $F_{si} = N_{si}/A_i$ ), and  $N_{si}$  is the number of all the streams found on  $A_i$ .

The well known measurements and correlations (Horton, Melton, Hack) of river basins<sup>10</sup> are anticipated very well and completely by the constructal structure displayed in Table III. The empirical correlations do not account for the size of the basin but the constructal approach does. The agreement improves as the size and complexity (i) of the basin increase. Horton’s empirical correlation of stream lengths indicates that  $R_L$  is a constant with a value between 1.5 and 3.5. Horton’s empirical correlation of stream numbers shows that  $F_B$  is a constant with a value between 3 and 5. Melton’s correlation states that  $F_s/D_\omega^2$  is a constant approximately equal to 0.7. Finally, Hack’s correlation indicates that the length of the mainstream  $L_{Mi}$  is proportional to  $A_i^b$ , where  $A_i$  is the basin area and  $b$  is an exponent between 0.5 and 0.56. In the last column of Table III, the value  $b=0.5$  was used to show in dimensionless terms that the constructal architecture also anticipates the trend correlated by Hack. In summary, in Table III the scaling laws of river basins are predicted based on pure theory.

Another approach to deducing tree-shaped drainage basins from the constructal law is based on the erosion model<sup>22</sup> presented in Fig. 5. The two flow regimes are seepage (Darcy flow) through regions of low permeability ( $K$ ), and seepage through high-permeability regions ( $K_p$ ) created by grains that have been removed. The drainage area  $A=HL$  and its shape  $H/L$  are fixed. The area is coated with a homogeneous porous layer of permeability  $K$ . The small thickness of the  $K$  layer (the dimension perpendicular to the plane  $H \times L$ ) is  $W$ , where  $W \ll (H, L)$ . An incompressible Newtonian fluid is

TABLE III. The theoretical structure of constructal river basins (Ref. 23).

$i$	$A_i/A_0$	$L_{Ti}/A_0^{1/2}$	$N_i$	$R_{Li}$	$R_{Bi}$	$D_{oi}A_0^{1/2}$	$F_{si}A_0$	$F_{si}/D_{oi}^2$	$L_{Mi}/A_i^{1/2}$
0	1	$\frac{1}{2}$	1	...	...	$\frac{1}{2}$	1	4	$\frac{1}{2}$
1	4	$\frac{7}{2}$	5	3	4	$\frac{7}{8}$	$\frac{5}{4}$	1.63	$\frac{3}{4}$
2	$4^2$	$\frac{35}{2}$	21	2	4	$\frac{35}{22}$	$\frac{21}{16}$	1.10	$\frac{3}{4}$
3	$4^3$	76	85	2	4	$\frac{76}{64}$	$\frac{85}{64}$	0.94	$\frac{3}{4}$
4	$4^4$	316	341	2	4	$\frac{316}{256}$	$\frac{341}{256}$	0.87	$\frac{3}{4}$
River basins				1.5–3.5 Horton	3–5 Horton			0.7 Melton	~1.4 Hack

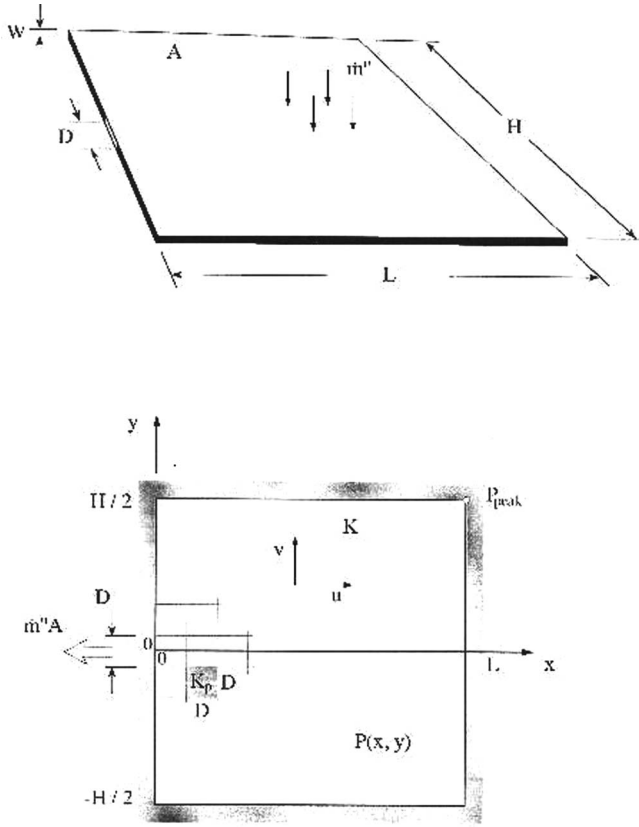


FIG. 5. Area-point flow in a porous medium with Darcy flow and grains that can be dislodged and swept downstream (Ref. 22).

pumped into one of the  $A$  faces of the  $A \times W$  parallelepiped, such that the mass flow rate per unit area is uniform,  $\dot{m}''[\text{kg}/\text{m}^2 \text{ s}]$ . The other  $A$  face and most of the perimeter of the  $H \times L$  rectangle are impermeable. The collected stream ( $\dot{m}''A$ ) escapes through a small port of size  $D \times W$  placed over the origin of the  $(x, y)$  system. The fluid is driven to this port by the pressure field  $P(x, y)$  that develops over  $A$ . The pressure field accounts for the effect of slope and gravity in a real river drainage basin, and the uniform flow rate  $\dot{m}''$  accounts for the rainfall.

The global resistance to this area-to-point flow is the ratio between the maximal pressure difference ( $P_{\text{peak}}$ ) and the total flow rate ( $\dot{m}''A$ ). The location of the point of maximal pressure is not the issue, although in Fig. 5 this position is clear. It is important to calculate  $P_{\text{peak}}$  and to reduce it at every possible turn by making appropriate changes in the internal structure of the  $A \times W$  system. Determinism results from invoking a single principle and using it consistently.

The physics principle that we invoke is this: the resistance to fluid flow is decreased at every time step through geometric changes in the internal architecture of the system. Changes in flow architecture are possible because finite-size portions (blocks, grains) of the system can be dislodged and ejected through the sink. The removable blocks are of the same size and shape (square,  $D \times D \times W$ ). The critical force (in the plane of  $A$ ) that is needed to dislodge one block is  $\tau D^2$ , where  $\tau$  is the yield shear stress averaged over the base area  $D^2$ . The yield stress and the length scale  $D$  are assumed known. They provide an erosion criterion and a useful esti-

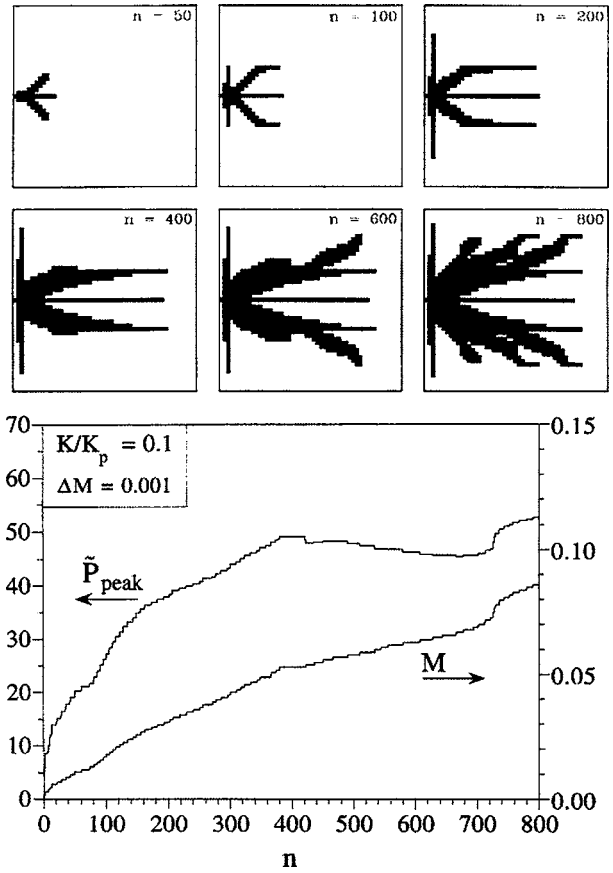


FIG. 6. The evolution (persistence, survival) of the tree structure when ( $K/K_p=0.1$ , the flow rate  $M$  is increased in steps  $\Delta M=0.001$ ) (Ref. 22).

mate of the order of magnitude of the pressure difference that can be sustained by the block. At the moment when one block is dislodged, the critical force  $\tau D^2$  is balanced by the net force induced by the local pressure difference across the block  $\Delta P$ , namely,  $\Delta P D W$ . The balance  $\tau D^2 \sim \Delta P D W$  suggests the pressure-difference scale  $\Delta P \sim \tau D / W$ , which along with  $D$  can be used for the purpose of nondimensionalizing the problem formulation: the dimensionless pressure difference is  $\tilde{P} = P / (\tau D / W)$ , and the intensity of the rainfall is described by the dimensionless number  $M = \dot{m}'' \nu D / (\tau K)$ .

A simple way to model erosion is to assume that the space vacated by the block is also a porous medium with Darcy flow except that the new permeability ( $K_p$ ) of this medium is sensibly greater  $K_p > K$ . This assumption is correct when the flow is slow enough (and  $W$  is small enough) so that the flow regime in the vacated space is Hagen-Poiseuille between parallel plates. The equivalent  $K_p$  value for such a flow is  $W^2/12$ . The availability of two dissimilar flow regimes ( $K_p \neq K$ ) is a necessary precondition for the formation of deterministic structures through flow-resistance minimization. The “glove” is the high-resistance regime ( $K$ ), and the “hand” is the low-resistance regime ( $K_p$ ): both regimes work toward minimizing the overall resistance.

The pressure  $\tilde{P}$  and the block-averaged pressure gradient increase in proportion with the imposed mass flow rate. In the scenario presented in Fig. 6, the dimensionless flow-rate parameter  $M$  is increased monotonically from one step to the next. Each step begins with the removal of the first block that

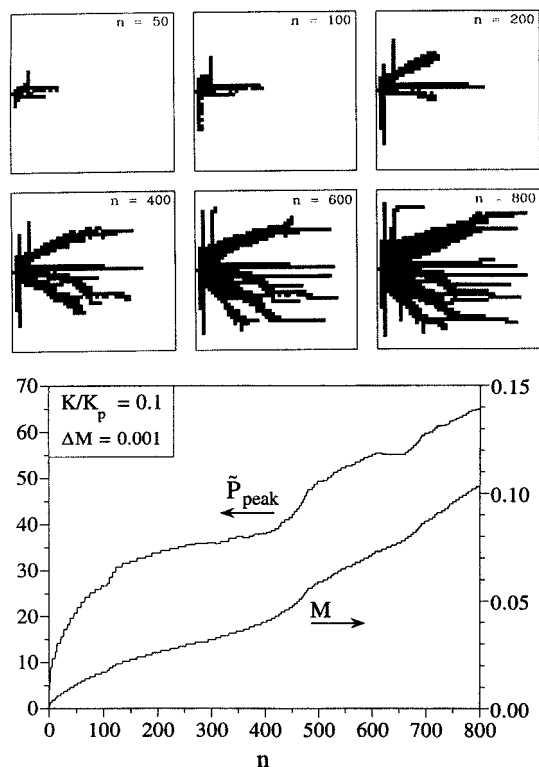


FIG. 7. The evolution (persistence, survival) of the tree structure in a random-resistance erodable domain ( $K/K_p=0.1$  and  $M$  increases in steps of  $\Delta M=0.001$ ) (Ref. 22).

can be dislodged by the flow rate  $M$ . Following the removal of the first block, the  $M$  value is held fixed, the pressure field is recalculated and the block removal criterion is applied again to the blocks that border the newly shaped  $K_p$  domain. To start the next step, the  $M$  value is increased by a small amount  $\Delta M$ . Figure 6 corresponds to a composite porous material with  $K/K_p=0.1$ . Simulations conducted for other  $K/K_p$  ratios show that the slenderness of the  $K_p$  channels and the interstitial  $K$  regions is dictated by the  $K/K_p$  ratio, that is, by the degree of dissimilarity between the two flow paths. Highly dissimilar flow regimes ( $K/K_p \ll 1$ ) lead to slender channels (and slender  $K$  interstices) when the overall area-to-point resistance is minimized. On the other hand, when  $K/K_p$  is close to 1, channels (fingers) do not form: the eroded region grows as a half disk.

The key result is that the removal of certain blocks of  $K$  material and their replacement with  $K_p$  material generate macroscopic internal *structure*. The generalizing mechanism is the minimization of flow resistance, and the resulting structure is deterministic: every time we repeat this process we obtain exactly the same sequence of images.

One difference between natural river drainage structures and the deterministic structures illustrated in Fig. 6 is the lack of symmetry in natural river trees. How do we reconcile the lack of symmetry and unpredictability of the finer details of a natural pattern with the deterministic resistance-minimization mechanism that led us to the discovery of the tree networks of Fig. 6? The answer is that the developing structure depends on two entirely different concepts: the gen-

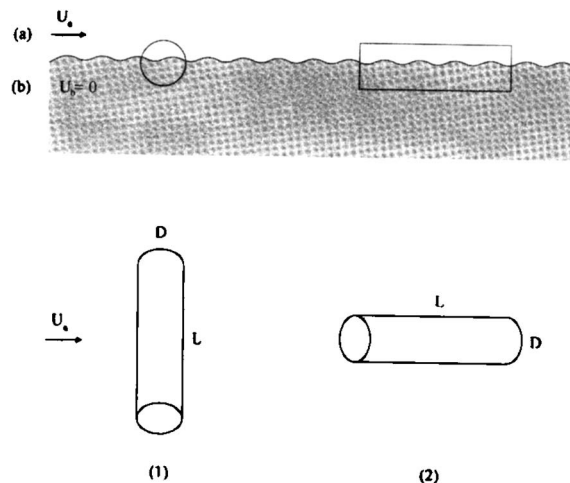


FIG. 8. Floating object at the interface between two fluid masses with relative motion (Ref. 6).

erating mechanism, which is deterministic, and the properties of the natural flow medium, which are not known accurately and at every point.

In the scenario shown in Fig. 7 it was assumed that the dislodging resistance that characterizes each removable block is distributed randomly over the basin area. This characteristic of river beds is well known in the field of river morphology. For the erosion process we chose the same composite system ( $K/K_p=0.1$ ) and  $M(n)$  function as in Fig. 6, in which  $M$  increased monotonically in steps of 0.001. The evolution of the drainage system is shown in Fig. 7. The emerging tree network is considerably less regular than in Fig. 6 and reminds us more of natural river basins. The unpredictability of this pattern, however, is due to the unknown spatial distribution of system properties, not to the configuration-generating principle (the constructal law), which is known. Further examples of generation of flow configuration in morphing fluid flow systems are treated in Refs. 24 and 25.

## D. Turbulent flow structure

A turbulent flow has “structure” because it is a combination of two flow mechanisms: viscous diffusion and streams (eddies). Both mechanisms serve as paths for the flow of momentum. According to the constructal law, the turbulent flow structure is the architecture that provides the most direct path for the flow of momentum from the fast regions of the flow field to the slow regions.<sup>1</sup>

This tendency of selecting the flow configuration so that momentum flows the easiest is illustrated in Fig. 8. An object (iceberg and tree log) floats on the surface of the ocean.<sup>6</sup> The atmosphere (a) moves with the wind speed  $U_a$ , while the ocean water (b) is stationary. If (a)+(b) form an isolated system initially far from equilibrium, the constructal law calls for the generation of flow configuration that brings (a) and (b) to equilibrium the fastest. The floating object is the lock-and-key mechanism by which (a) transfers momentum to (b). The extreme configurations of this mechanism are labeled (1) and (2). The forces with which (a) pulls (b) are

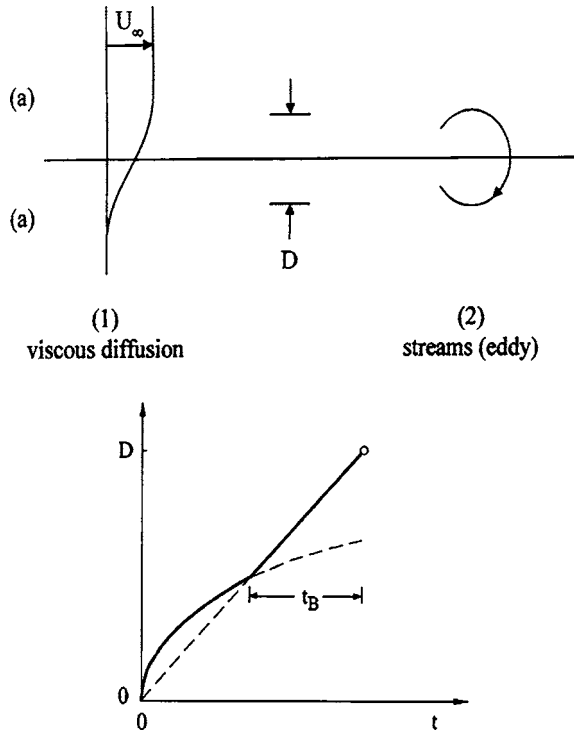


FIG. 9. The two momentum-transfer mechanisms that compete at the interface between two flow regions of the same fluid (Ref. 6).

$$F_1 \sim LDC_D \frac{1}{2} \rho_a U_a^2, \quad F_2 \sim D^2 C_D \frac{1}{2} \rho_a U_a^2, \quad (4)$$

where the drag coefficient  $C_D$  is a factor of order 1. The selected configuration must be (1), because  $F_1 > F_2$  when  $L > D$ . This is confirmed by all objects that drift on the ocean: icebergs, debris, abandoned ships, etc.

The turbulent eddy is analogous to the floating object example: in the case of the eddy the momentum access is maximized between two regions of the same flowing fluid. Figure 9 shows the shear flow between fast and slow regions of fluid (a). Configuration (1) is the laminar shear flow (viscous diffusion), where the shear stress at the (a)-(a) interface is  $\tau_1 \sim \mu U_\infty / D$ . Configuration (2) is the eddy flow: the wrin-

gling, mixing and thickening of the shear layer by rolling the near-interface fluid. The roll has the peripheral speed  $U_\infty$  and transfers horizontal momentum in the downward direction [from (a) to (a)] at the rate  $(\rho D U_\infty) U_\infty$ . The apparent shear stress at the interface is  $\tau_2 \sim \rho D U_\infty^2 / D$ . Rolls (eddies) are a necessary constructural feature of the prevailing flow architecture when  $\tau_2 > \tau_1$ , which yields  $U_\infty D / \nu > 1$ . More precise evaluations of  $\tau_1$  and  $\tau_2$ , which are substituted into  $\tau_2 > \tau_1$ , yield the local Reynolds number criterion for the formation of the first eddies:

$$Re_l = \frac{U_\infty D}{\nu} > O(10^2). \quad (5)$$

This prediction is supported convincingly by the laminar-turbulent transition criteria reviewed in Table IV. The traditional criteria are stated in terms of critical numbers that range from 30 to  $4 \times 10^{12}$ . The  $Re_l$  equivalents condense this information and agree with  $Re_l \sim 10^2$  at transition.

The competition between viscous diffusion and organized movement (rolls) is shown graphically<sup>1,6,17</sup> in the lower part of Fig. 9. At small times, the thickness of the shear zone  $D$  grows very fast, as  $t^{1/2}$ . At longer times, the faster growth is by organized motion (rolling, eddies), when  $D$  is proportional to  $t$ . The intersection of the two curves dictates the buckling time  $t_B$ , which is the first heartbeat of turbulence—the birth of the first eddy. This event is equivalent to knowing  $Re_l$  of Eq. (5). During the next  $t_B$  interval (shown in Fig. 9), the first eddy completes its first roll, after which coalescence (pairing) and larger rolls and longer rolling times follow. The entire large scale structure (the lengths and the times) of the turbulent mixing region is predicted from Eq. (5) and Fig. 9, without recourse to empiricism.<sup>1,6,17</sup>

The main theoretical development is that the constructural law accounts for the occurrence of eddies. Here the eddy structure is deduced, not assumed (the eddy is not the result of an assumed “disturbance”). Each eddy is an expression of the optimal balance between two momentum transport mechanisms, in the same way that every rivulet is in balance with the seepage across the area allocated to the rivulet.

TABLE IV. Traditional critical numbers for transitions in several key flows and the corresponding local Reynolds number (Ref. 17).

Flow	Traditional critical number	Local Reynolds number
Boundary-layer flow over flat plate	$Re_x \sim 2 \times 10^4 - 10^6$	$Re_l \sim 94 - 660$
Natural convection boundary layer along vertical wall with uniform temperature ( $Pr \sim 1$ )	$Ra_y \sim 10^9$	$Re_l \sim 178$
Natural convection boundary layer along vertical wall with constant heat flux ( $Pr \sim 1$ )	$Ra_{y^*} \sim 4 \times 10^{12}$	$Re_l \sim 330$
Round jet	$Re_{nozzle} \sim 30$	$Re_l \geq 30$
Wake behind long cylinder in cross flow	$Re \sim 40$	$Re_l \geq 40$
Pipe flow	$Re \sim 2000$	$Re_l \sim 500$
Film condensation on a vertical wall	$Re \sim 450$	$Re_l \sim 450$

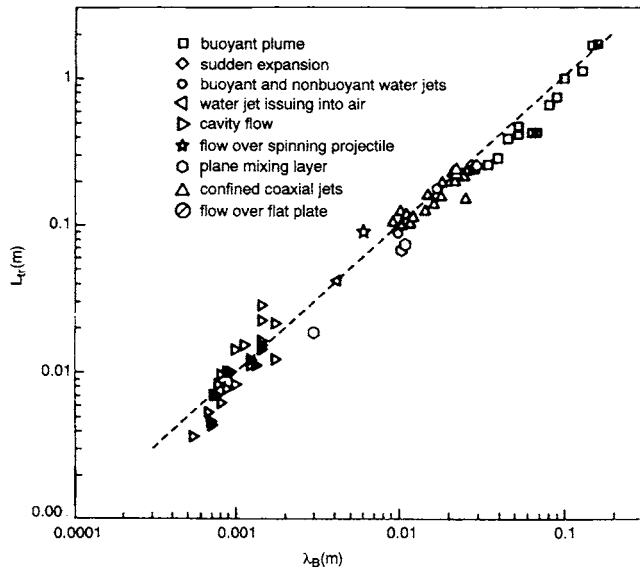


FIG. 10. The universal proportionality between the length of the laminar section and the buckling wavelength in a large number of flows (Ref. 17).

The support for the theoretical view of turbulence as a constructal configuration-generation phenomenon is massive. Table IV is one example of how an entire chapter of fluid mechanics is replaced by a single theoretical formula, Eq. (5). Another example is Fig. 10, which shows a large number of measurements of the laminar length ( $L_l$ ) in the best known flow configurations, versus the buckling wavelength ( $\lambda_B$ ) in the transition zone. All the data are correlated by the line  $L_l/\lambda_B \sim 10$ . It was shown in Ref. 17 that this proportionality is a direct consequence of Eq. (5). Other features of turbulent structure that have been deduced from the constructal law are the wedge shape (self-similar region) of turbulent shear layers, jets and plumes, and the Strouhal number associated with vortex shedding.<sup>1,18</sup>

### E. Coalescence of flowing solid packets

Many other forms of natural organization can be predicted from the flow access-maximization point of view of constructal theory. Least expected are the patterns exhibited by solids. One such phenomenon is the coalescence (clumping) of solid particles that are entrained by a fluid flow.<sup>1</sup> Consider two such granules—for example, two balls of diameter  $D_1$  and density  $\rho$ , such that their total mass is  $m = 2\rho(\pi/6)D_1^3$ . The drag force felt by each ball is  $F_D = C_D(\pi/4)D_1^2 \frac{1}{2} \rho_f U^2$ , where  $\rho_f$  is the density of the medium (e.g., gas) that fills the space, and  $U$  is the relative velocity between ball and medium. For simplicity, assume that the Reynolds number is sufficiently large such that the drag coefficient  $C_D$  is a constant of order 1. The drag force experienced by the total mass  $m$  is

$$F_1 = 2F_D = \frac{\pi}{4} C_D D_1^2 \rho_f U^2. \quad (6)$$

Can the two masses reduce their resistance to travel? In other words, can the solid spread faster and farther through space? Two balls fused into one larger ball encounter a smaller resistance than when they travel separately. Mass

conservation dictates that the diameter of the larger ball is  $D_2 = 2^{1/3} D_1$ . The drag force on this larger ball,

$$F_2 = C_D \frac{\pi}{4} D_2^2 \frac{1}{2} \rho_f U^2 \quad (7)$$

is smaller than in the original configuration,  $F_2/F_1 = 2^{-1/3} = 0.794$ . Given enough time, two masses will coalesce into a larger mass, in a process that repeats itself many times. We see it everywhere in space, for example, during large-scale explosions. The debris does not expand uniformly (spherically) outward; rather, it comes together into several radial streamers, each with a round cross-section because the solid streamer drags a turbulent jet of air (cf. Sec. II D).

### F. Cracks

Another solid pattern is visible in the cracking of mud. Soil exposed to the sun and the wind becomes drier, shrinks superficially, and develops a network of cracks. The loop of the network has a characteristic length scale. The loop is round, more like a hexagon or square, not slender. The loop is smaller when the wind blows harder—that is, when the drying rate is higher. These features have been predicted<sup>26</sup> based on constructal theory by maximizing the mass transfer rate between wet soil and ambient, which is equivalent to minimizing the overall drying time. For example, the characteristic length scale of the loop varies inversely with the wind speed.

### G. Dendritic crystals

The dendritic crystals formed during rapid solidification are another class of naturally ordered solid shapes.<sup>1</sup> Snowflakes are tree-shaped like the river basins, but the ice is solid: what flows through such trees? The answer is that heat flows, and the reason for the dendritic architecture of snowflakes is the same as for river basins: the maximization of access for the currents that flow. The latent heat released at the solid-liquid interface during solidification must be conducted into the metastable liquid that surrounds the solid. The solidification is “rapid” because at every point in time the nonequilibrium system selects the configuration through which heat flows fastest. At short times, the most effective configuration to generate solid and warm up the liquid (subcooled) is the sphere. The radius of the sphere increases as  $t^{1/2}$ . After a critical time  $t_c$ , which is analogous to the transition time expressed by Eq. (5) and Fig. 9, the more effective way to transfer heat is a needle that grows at constant speed along its axis. In this second scenario, the radius of the region brought to equilibrium by the solidification process increases as  $t$ . At long times, the more effective configuration is the needle not the sphere.

The competition between spherical growth and needle growth repeats itself after each characteristic time  $t_c$ . The result is a solid structure made of needles of characteristic length, which are fossils of the volumetric flow of heat that once existed. Snowflakes are plane, and not cylindrical and spherical, for the same reason: the rate of volumetric solidi-

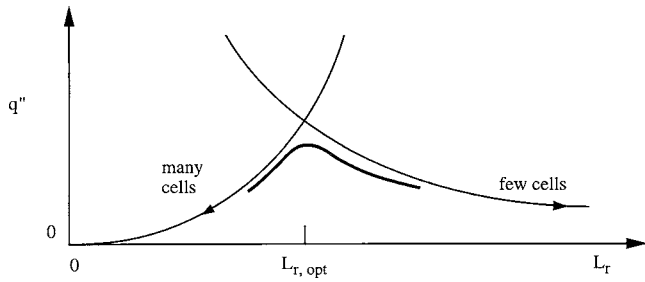


FIG. 11. Bénard convection as a constructal design: the intersection of the many-cell and few-cell asymptotes.

fication is the greatest when the dendrite is plane. Further work on the optimization of snow morphology is reported in Ref. 27.

**H. Global circulation and climate**

The prediction of turbulent flow structure (rolls, eddies, Sec. II D) was extended to fluid layers and fluid-saturated porous media heated from below.<sup>28</sup> This extension accomplished two things: (i) it established the connection between the constructal law and Malkus’ hypothesis<sup>29</sup> that in the Bénard convection the global heat transfer rate is maximized, and (ii) it predicted all the known characteristics of the Bénard convection. The method is outlined in Fig. 11. The global heat transfer rate ( $q''$ ) from the bottom to the top of the fluid layer was estimated analytically in the two extremes of (a) many cells (small  $L_r$ ) and (b) few cells (large  $L_r$ ), where  $L_r$  is the horizontal length scale of the roll. It was shown that asymptotes (a) and (b) intersect:  $q''$  decreases monotonically as  $L_r$  decreases when  $L_r$  is small, and  $q''$  decreases as  $L_r$  increases when  $L_r$  is large. The intersection of asymptotes method<sup>6,12,17</sup> delivered the thickness of the roll that vehicles maximum heat transfer across the layer. From this prediction followed the critical Rayleigh number  $Ra_c$  of order of  $10^3$  for the onset of convection, and the Nusselt number of order  $Ra^{1/3}$  when  $Ra \gg Ra_c$ . Here  $Ra$  is the Rayleigh number based on the vertical dimension of the fluid layer, and on the bottom-top temperature difference. For a horizontal porous layer saturated with fluid, the same theory predicts a critical Rayleigh number  $Ra_{p,c} = 12\pi = 37.3$  (instead of the stability-analysis result  $4\pi^2 = 39.5$ ), and a proportionality between Nusselt number and  $Ra_p^{2/3}$ , where the porous medium Rayleigh number is based on vertical dimension, bottom-top temperature difference and porous medium permeability.

This approach was taken to even larger scales to predict based on pure theory the main features of terrestrial atmospheric and oceanic circulation.<sup>30,31</sup> Empirical models coupled with the hypothesis that the rate of entropy production is maximized began with Malkus hypothesis.<sup>29</sup> Examples and reviews of such models are available in Refs. 32–38 (See also Sec. VI). The approach based on the constructal law derives the main features of the flow architecture from the maximization of the flow access performance of the whole system under the existing constraints. According to thermodynamics terminology,<sup>1</sup> the Earth is a closed system, not an open system. It is not an isolated system. The nonuni-

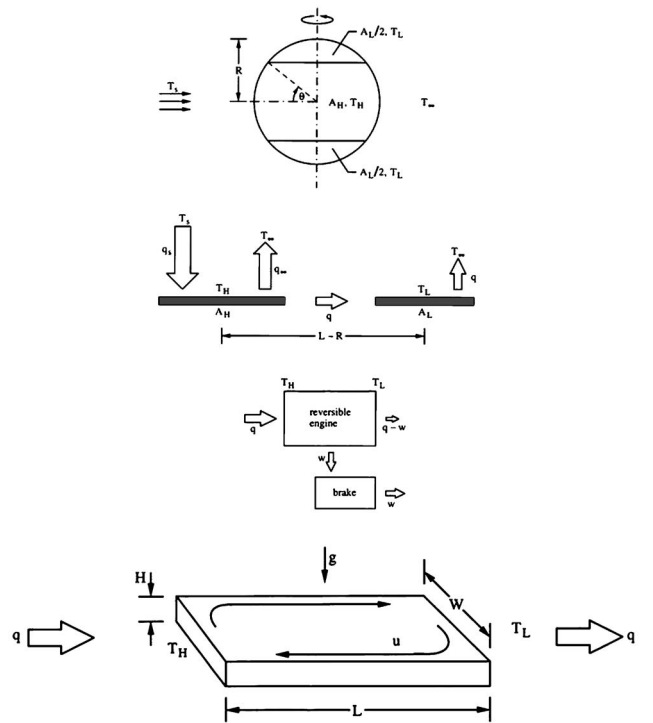


FIG. 12. Earth model (Refs. 30 and 31) with equatorial ( $A_H$ ) and polar ( $A_L$ ) zones, and convective heat current carried by natural convection loops that constitute the brake to which the Sun-Earth- Universe engine is connected (see also Fig. 33).

form heating of the Earth’s surface and atmosphere drives the Earth circulation. The purpose of the circulation (the objective of any flow with configuration) is to provide maximum access to the currents that flow, in this case to transfer heat from the equatorial zone to the polar caps. The zones and caps are organized in such a way that they perform this transport in the most efficient way, which is the one that maximizes the heat flow or, alternatively, by the flow structure that minimizes the resistance to the global heat flow.

The method consists of viewing the Sun-Earth- Universe assembly as an extraterrestrial power plant the power output of which is used for the purpose of forcing the atmosphere and hydrosphere to flow, Fig. 12. This circulation destroys all the power generated by the Sun-Earth- Universe power plant: the maximization of thermodynamic performance (power output) in the power plant becomes equivalent to the maximization of power dissipation in the atmospheric and oceanic circulation. We return to this equivalence in Sec. VI. The power plant models that have been proposed and optimized are listed in Refs. 1 and 39–42.

A spaceship, or the Earth, may be viewed as a closed system having two surfaces, a hot surface of area  $A_H$  and temperature  $T_H$ , which is heated by the sun, and a cold surface ( $A_L, T_L$ ) cooled by radiation to the universe. On a spaceship, the collector ( $A_H$ ) and radiator ( $A_L$ ) are the object of design. In the modeling of wind generation on Earth, the surfaces  $A_H$  and  $A_L$  represent the daily illuminated and dark hemispheres, or the time-averaged equatorial and polar zones. In all cases, the total radiation heat transfer surface is fixed,  $A_H + A_L = A$ . Global finiteness constraints of this type play a central role in constructal theory. In Refs. 30 and 31

the model of Fig. 12 was used to optimize the latitude of the boundary between the Hadley and the Ferrel cells, and the boundary between the Ferrel and the Polar cells. The average temperature of the Earth surface, the convective conductance in the horizontal direction, as well as other parameters defining the latitudinal circulation, also match the observed values.

The constructal law was also invoked in the analysis of atmospheric circulation at the diurnal scale, where the heat transport is optimized against the Ekman number. Even though this second optimization is based on very different variables, it produces practically the same results for the Earth surface temperature and the other variables. The Earth averaged temperature difference between day and night was found to be approximately 7 K, which matches the observed value.

The accumulation of coincidences between theoretical predictions and natural facts adds weight to the claim that the constructal law is a law of nature.

### III. ANIMATE FLOW CONFIGURATIONS

The phenomenon of generation of flow configuration is everywhere in living systems. Tree-shaped flow architectures emerge in animal design because they are the easiest way to flow between an infinity of points (volume, area) and one point. Human lungs, kidneys, vascularized tissues and the nervous system are examples of tree architectures that have been treated from the point of view of constructal theory.<sup>1,6,43</sup> In this section we review a series of theoretical developments in which the constructal law and constructal architectures such as trees have led to astonishingly simple and direct predictions of the scaling laws of animal design, across the board, over all known body-mass scales. This treatment is based on the broad view that the principles that apply to flow systems in physics and engineering must also apply to biological flow systems.<sup>44–60</sup>

#### A. Body heat loss versus body size

Larger animals have larger metabolic rates, or larger rates of body heat loss ( $q$ ). Measurements of  $q$  plotted against the body mass ( $M_b$ ) of animals in size range of  $10^{-2} \text{ kg} < M_b < 10^2 \text{ kg}$  reveal a correlation<sup>44</sup> of the type  $q \sim M_b^n$ , where the empirical exponent  $n$  is approximately 0.75. This empirical correlation is the best known and most challenging to predict in animal design. In this section we outline two recent attempts to explain this trend, one is purely theoretical<sup>51</sup> and the other based on a three-assumption model.<sup>53</sup> The earlier attempt was Rubner's heat transfer model:<sup>1</sup> the convective heat loss to the ambient is proportional to the body surface, therefore the heat loss (or metabolic rate) must be proportional to the body length scale ( $V^{1/3}$ ) squared, where  $V$  is the body volume. According to Rubner,  $q$  should increase as  $V^{2/3}$ , or  $M_b^{2/3}$ .

The heat transfer model was discredited by more recent  $q$ - $M_b$  data from birds and mammals, which suggest an exponent closer to 3/4 than 2/3. For this reason, heat transfer was not included in the model of West *et al.*<sup>53</sup> It was included in the constructal-theory argument of Ref. 51 and Fig.

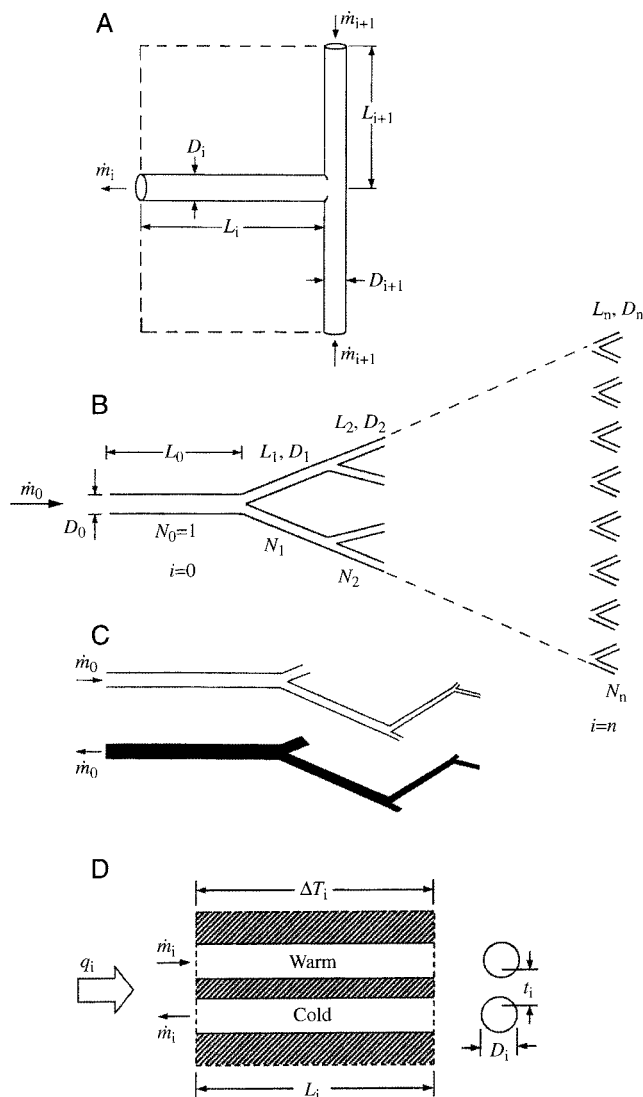


FIG. 13. The construction of the tree of convective heat currents: (A) the constrained optimization of the geometry of a T-shaped construct; (B) the stretched tree of optimized constructs; (C) the superposition of two identical trees oriented in counterflow; and (D) the convective heat flow along a pair of tubes in counterflow (Ref. 6).

13, which is based on the minimization of body heat loss, and the minimization of blood pumping power. The minimization of pumping power yields the constructal fluid tree:<sup>1,5,6</sup> this can be derived more succinctly by optimizing a planar construct consisting of a T-shaped junction,<sup>61</sup> Fig. 13(A). For simplicity, assume right angles and Hagen-Poiseuille flow with constant properties in every tube. The stream  $\dot{m}_i$  encounters the flow resistance of two  $L_{i+1}$  tubes in parallel, which are connected in series with one  $L_i$  tube. When the resistance is minimized by fixing the total tube volume, we find the Hess-Murray law<sup>46</sup>  $D_{i+1}/D_i = 2^{-1/3}$ , which is independent of the tube lengths ( $L_i, L_{i+1}$ ) and the relative position of the three tubes. Next, we optimize the lengths when the space allocated to the construct is fixed,  $2L_{i+1}L_i = \text{const}$ . This yields the optimal ratio  $L_{i+1}/L_i = f = 2^{-1/3}$ , where the smallest length scale is labeled  $i=n$ , and the largest  $i=0$ .

The trees of blood vessels are an architectural feature under the skin, but not the only one. The other is the *superposition* of the arterial and venous trees, so closely and regu-

larly that tube  $i$  of one tree is in counterflow with tube  $i$  of the other [Figs. 13(C) and 13(D)]. This is a *thermal insulation* feature. The arterial stream is warmer than the venous stream: heat flows transversally, from stream to stream. Because the enthalpy of the warmer stream is greater than that of the colder stream, the counterflow convects longitudinally the energy current  $q_i = \dot{m}_i c_p \Delta T_{t,i}$ , where  $c_p$  is the specific heat of blood, and  $\Delta T_{t,i}$  is the stream-to-stream temperature difference at level  $i$ . It was shown<sup>62,63</sup> that such a counterflow sustains a longitudinal temperature gradient  $\Delta T_i/L_i$  and that the convective energy current is proportional to this gradient:

$$q_i = \left[ \frac{(\dot{m}_i c_p)^2}{h_i p_i} \right] \frac{\Delta T_i}{L_i}, \quad (8)$$

where  $h_i$  is the overall stream-to-stream heat transfer coefficient and  $p_i$  is the perimeter of contact between the two streams. The stream-to-stream thermal resistance  $h_i^{-1}$  is the sum of two resistances: the thermal resistance posed by the fluid present in the duct ( $\sim D_i/k_f$ , where  $k_f$  is the fluid thermal conductivity), plus the resistance to heat transfer through the solid tissue that separates two tubes ( $\sim t_i/k$ , where  $D_i$  is the diameter and  $k$  is the tissue thermal conductivity;  $t_i$  is defined in Fig. 13(D):  $t_i$  is the average thickness of the tissue that separates two adjacent  $D_i$  tubes). Even when the tubes touch,  $t_i$  is of the same order as  $D_i$ . In addition, because  $k_f \sim k$ , we conclude that  $h_i \sim k/D_i$ , and Eq. (8) becomes

$$\Delta T_i \sim \frac{q_i L_i k}{\dot{m}_i^2 c_p^2}. \quad (9)$$

The double-tree fluid structure is a single tree of convective heat leakage with zero net mass flow. The convective tree stretches from the core temperature of the animal (at  $i=0$ ) to the skin temperature. The latter is registered in many of the elemental volumes ( $i=n$ ) that are near the skin. The many counterflow pairs of the two fluid trees sustain the overall temperature difference  $\Delta T$ :

$$\Delta T = \sum_{i=0}^n \Delta T_i \sim \frac{q_0 k}{\dot{m}_0^2 c_p^2} \sum_{i=0}^n N_i L_i. \quad (10)$$

In going from Eq. (9) to Eq. (10), we used the continuity relations for fluid flow ( $N_i \dot{m}_i = \dot{m}_0 = \text{const}$ ), and heat flow ( $N_i q_i = q_0, \text{const}$ ). Recalling the  $L_{i+1}/L_i$  constant  $f$ , we substitute  $L_i = L_0 f^i$ ,  $L_n = L_0 f^n$  and  $N_i = 2^i$  into Eq. (10):

$$q_0 \sim \left( \frac{q_0}{\dot{m}_0} \right)^2 \left\{ \frac{k L_n f^{-n} [(2f)^{n+1} - 1]}{c_p^2 \Delta T (2f - 1)} \right\}. \quad (11)$$

The right side has quantities that are constant, and quantities that depend on  $n$  (the number of construction steps). The ratio  $q_0/\dot{m}_0$  is independent of body size ( $n$ ) because both  $q_0$  and  $\dot{m}_0$  are proportional to the metabolic rate. The volume inhabited by the tree is estimated by considering the stretched tree as a cone in Fig. 13(B). The base of the cone (at  $i=n$ ) has an area of size  $N_n L_n^2 \sim 2^n L_n^2$ . The height of the cone is of the same order as the sum of all the tube lengths,  $L_0 + L_1 + \dots + L_n = L_0(1 - f^{n+1})/(1 - f)$ , and the volume scale is

$$V \sim L_n^2 \left( \frac{2}{f} \right)^2 \left( \frac{1 - f^{n+1}}{1 - f} \right). \quad (12)$$

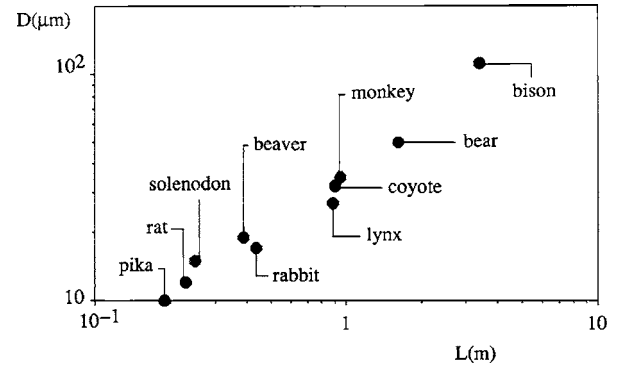


FIG. 14. The allometric law for animal hair strand diameter and body length scale.

The relationship between metabolic rate and total volume is obtained by eliminating  $n$  between Eqs. (11) and (12). The result is visible in closed form if  $n$  is sufficiently large so that  $(2f)^{n+1} \gg 1$  in Eq. (11), and  $f^{n+1} \ll 1$  in Eq. (12). In this limit  $q_0$  is proportional to  $2^n$ , and  $V$  to  $(2/f)^n$ . From this follows:

$$q_0 = (\text{const}) V^{3/4}. \quad (13)$$

It can be verified numerically that Eq. (13) also holds for small  $n$ . In conclusion, the proportionality between metabolic rate and body size raised to the power of 3/4 is predictable from pure constructal theory.

The allometric law (13) was also derived in Ref. 53, which is a model based on at least three *ad hoc* assumptions.

- (i) The existence of “space-filling fractal-like branching pattern,” i.e., a tree.
- (ii) The final branch of the network is a size-invariant unit.
- (iii) The energy required to distribute resources is minimized.

These three features were already present in 1996 constructal theory,<sup>1-5</sup> not as assumptions to improve a model and make it work, but as invocations of a single principle: the constructal law. The overlap is described in Ref. 64. Specifically, (iii) is covered by the constructal law, (i) is the tree-flow architecture that in constructal theory is deduced from the constructal law, and (ii) is the smallest-element scale that is fixed in all the constructal tree architectures. To repeat, in constructal theory the tree-shaped flow is a discovery, not an observation, and not an assumption.

Additional support for the constructal theory of body heat loss comes from the allometric laws of the design of the hair coats of animals, such as the proportionality between the hair strand diameter and the animal body length scale raised to the power of 1/2 (Fig. 14). This allometric law was predicted<sup>65,66</sup> by minimizing the body heat loss through the hair coat. The 1/2 exponent was predicted for both natural convection and forced convection. Another common feature of animal hair coats is the porosity, which is high and nearly constant (between 0.95 and 0.99) for all animal sizes.<sup>14,67</sup> This feature was predicted by minimizing the combined heat loss by conduction and radiation through the hair air coat.

Constructal theory predicts not only the 3/4 exponent for Eq. (13) but also the gradual decrease of this exponent as the body size decreases. The 3/4 exponent is valid at the limit where the body heat loss is impeded primarily by the convective resistance posed by the blood counterflow of perfectly matched tube pairs [Fig. 13(B)]. Heat-loss paths are in general more complicated.<sup>6,51</sup> The convective thermal resistance posed by the trees in counterflow ( $R_1$ ) resides inside the animal. This resistance runs in parallel with a second internal resistance ( $R_2$ ) associated with the conductive heat leak through the tissue. On the outside of the animal the heat current flows through the convective resistance ( $R_3$ ) associated with the body surface exposed to the ambient (air and water). The conductive resistance  $R_2$  is proportional to the body length scale  $V^{1/3}$  divided by the body surface scale  $V^{2/3}$ ; hence  $R_2 \sim V^{-1/3}$ . The convective tree resistance  $R_1$  is proportional to  $V^{-3/4}$ . The ratio  $R_2/R_1 \sim V^{5/12}$  shows that  $R_2$  becomes progressively weaker (i.e., the preferred path) as the body size decreases: in that limit the exponent in the power law between heat loss and body size becomes 1/3. In other words, from constructal theory we should expect a gradual decrease in the power-law exponent as the body size decreases.

**B. Breathing and heartbeating**

Constructal theory anticipates the proportionality between breathing (or heartbeating) time and body size raised to the power of 1/4. Reference 4 showed that the pumping power required by the heart for blood circulation and the thorax for breathing is minimal if (a) The flow is intermittent (in and out, on and off), and (b) The “in” interval ( $t_1$ ) is of the same order of magnitude as the “out” interval ( $t_2$ ).

Results (a) and (b) are important because they come from pure theory (the constructal law), not from observations. Result (a) means that intermittency is a constructal design feature, such as the tree architecture and the round duct. The optimal time scale ( $t_{1,2} \sim t$ ) is

$$t \sim \left( \frac{AD^{1/2}\Delta C}{\dot{m}} \right)^2, \tag{14}$$

where  $A$  is the total internal contact area of all the tubes of the tree,  $D$  is the mass diffusivity,  $\Delta C$  is the concentration difference that drives the mass transfer process, and  $\dot{m}$  is the total mass flow rate of the tree (blood and air). The flow rate  $\dot{m}$  is the total mass flow rate of the tree (blood and air). The flow rate  $\dot{m}$  is proportional to the metabolic rate of the animal.

Equation (14) shows that in order to predict  $t$  as a function of body mass ( $M_b$ ) we need expressions for  $\dot{m}(M_b)$  and  $A(M_b)$ . From the optimized tree of convective currents we obtained Eq. (13), or

$$\dot{m} \sim M_b^{3/4}. \tag{15}$$

To predict the relation  $A(M_b)$ , we argue that the thickness of the tissue penetrated by mass diffusion during the breathing or heartbeating time  $t$  is proportional to  $t^{1/2}$ . The body volume (or mass) of the tissue penetrated by mass diffusion during this time obeys the proportionality  $M_b \sim At^{1/2}$ . Eliminating

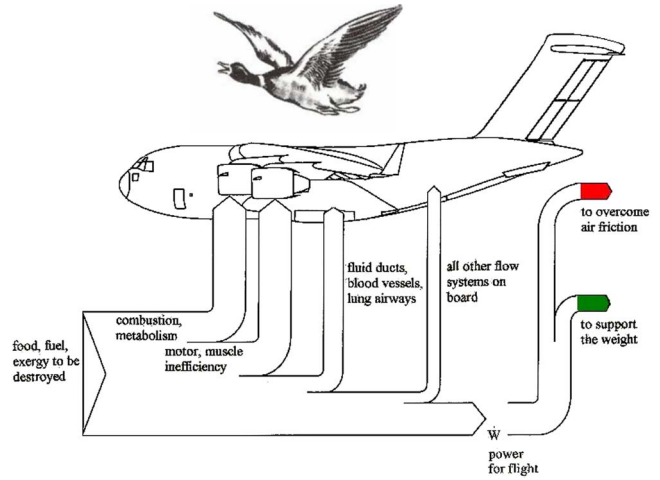


FIG. 15. (Color online) The distributed destruction of food or fuel exergy during flight.

nating  $t$  between  $M_b \sim At^{1/2}$  and  $t \sim (A/\dot{m})^2$ , and using Eq. (15) we conclude that the contact area should be almost proportional to the body mass,

$$A \sim M_b^{7/8}. \tag{16}$$

Finally, the proportionalities (14)–(16) mean that

$$t \sim M_b^{1/4}. \tag{17}$$

This allometric law is supported convincingly by the large volume of observations accumulated in the physiology literature.<sup>44</sup>

**C. Flying**

The animal design principles reviewed so far are relevant across the board, from biology to engineering. This point is pressed with vigor by the aircraft sketched in Fig. 15: if the word “fuel” is replaced by “food,” then the same drawing is valid for a bird, and reveals how the exergy liberated by food is destroyed by all the currents that flow

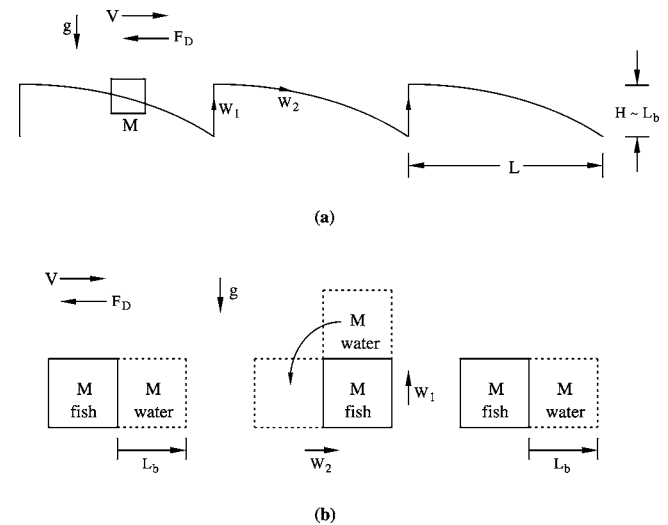


FIG. 16. (A) The periodic trajectory of a flying animal and (B) the cyclical progress of a swimming animal.

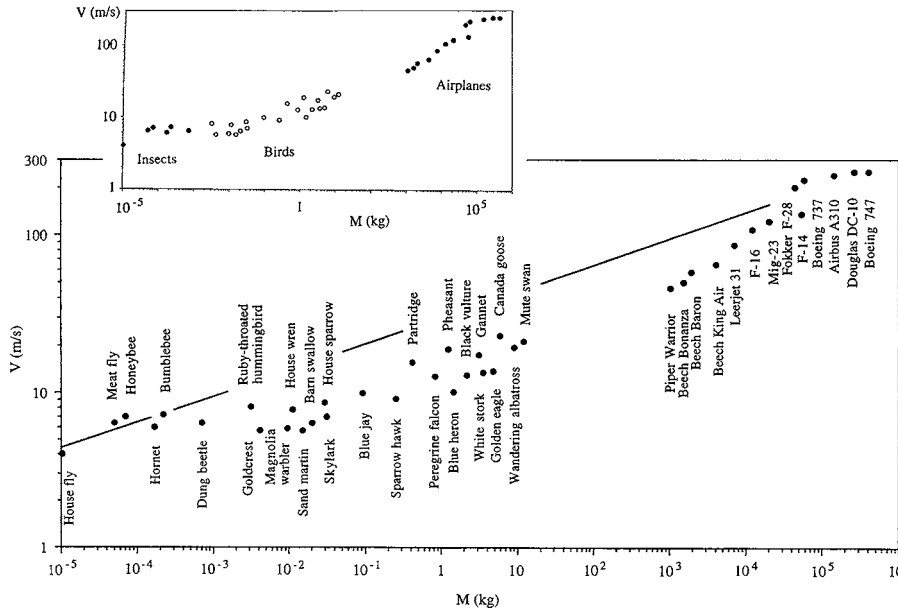


FIG. 17. The flying speeds of insects, birds and airplanes, and their theoretical constructal speed (Ref. 6).

around and through the animal. The food or fuel exergy is destroyed completely by currents that overcome resistances.

The flying system becomes “more fit” when the total destruction of exergy is minimized: more body mass flown, to longer distances. The flock of wild geese migrating from Alaska to the Amazon is just like the Danube and the Gulf Stream: more water mass carried with less resistance, i.e., faster and for longer distances. The mechanisms that destroy food exergy (e.g., air friction) cannot be minimized individually and eliminated, because each such mechanism serves the flying body as a whole. This was illustrated in most general terms<sup>6</sup> by minimizing the work (food exergy  $W$ ) destroyed per distance traveled ( $L$ ). The loss  $W$  has two components, vertical and horizontal. The vertical loss ( $W_1 \sim MgH$ ) is the work done in order to lift the body that had fallen to the vertical distance  $H$  during the free-fall time  $t \sim (H/g)^{1/2}$ . During the same time, the work spent on overcoming drag is  $W_2 \sim F_D L$ , where  $\rho_a$  is the air density, and the drag force is  $F_D \sim \rho_a V^2 L_b^2 C_D$ , with  $C_D \sim 1$ . The linear dimension of the body is  $L_b$ , the body mass is  $M$ , and the corresponding body density is  $\rho_b \sim M/L_b^3$ . Cycles in which  $W_1$  and  $W_2$  alternate in order to maintain the cruising speed at constant altitude are sketched in Fig. 16(A). The total loss per distance traveled is

$$\frac{W}{L} \sim \underbrace{\frac{MgH}{V(H/g)^{1/2}}}_{\text{vertical loss}} + \underbrace{\frac{\rho_a V^2 L_b^2}{V}}_{\text{horizontal loss}}. \quad (18)$$

The altitude increment achieved during each flapping stroke ( $H$ ) is dictated by the wing length scale, which is the length scale of the flying body  $H \sim L_b$ . By minimizing  $W/L$  we find the optimal cruising speed

$$V_{\text{opt}} \sim \left( \frac{\rho_b}{\rho_a} \right)^{1/3} g^{1/2} \rho_b^{-1/6} M^{1/6}. \quad (19)$$

Flying animals and machines are represented by the scales  $\rho_a \sim 1 \text{ kg m}^{-3}$  and  $\rho_b \sim 10^3 \text{ kg m}^{-3}$ , such that Eq. (19) becomes  $V_{\text{opt}} \sim 30M^{1/6}$ , where  $V_{\text{opt}}$  is expressed in  $\text{m s}^{-1}$  and  $M$  in kilograms. This theoretical speed is shown as a straight line in Fig. 17, next to the flying speed data taken from extensive compilations (Tennekes<sup>68</sup> and references therein; we return to the compilation of flying data after Secs. III D and III E). The agreement between the line and the data is remarkable, in view of the body model with one scale ( $L_b$ ). Insects, birds, and airplanes have multiple length scales, and this may explain why some of the data fall above or below the line.<sup>52</sup>

Agreement over such a wide diversity of sizes and types of flying flow systems shows that the constructal law unites the designs of all the flying systems, the animate with the engineered. This is stressed by other features of Fig. 17. Small animals (insects and hummingbirds) flap their wings all the time, and their engine propellers (the wings) also provide the lift. In this limit of small mass, the motor and the lift functions are performed by a single structure: the wings. At the other end of the body-mass scale, large masses (aircraft) fly with separate motor and lift structures. The lift is provided by the wings proper, and the motor (thrust) by a different set of wings—the blades of the turbofan engine. Between the “fully integrated” and “separate” motor and lift we find the “almost separate” distribution of motor and lift functions. We see this in the V-shaped flocks of migratory birds. The goose is the motor when it flies at or near the tip of the V formation; when it is not, the goose surfs on the waves generated by the geese working in front. Pterosaurs are also in-between. Their motor and lift functions were almost separate: they flapped their wings rarely, and glided most of the time under the hot sun.<sup>69</sup>

The wing flapping frequency that corresponds to the constructal speed [Eq. (19)] is  $t^{-1} \sim (g/L_b)^{1/2}$ , which is the formula shown for flyers in Fig. 18(B). The dimensionless frequency is the Strouhal number

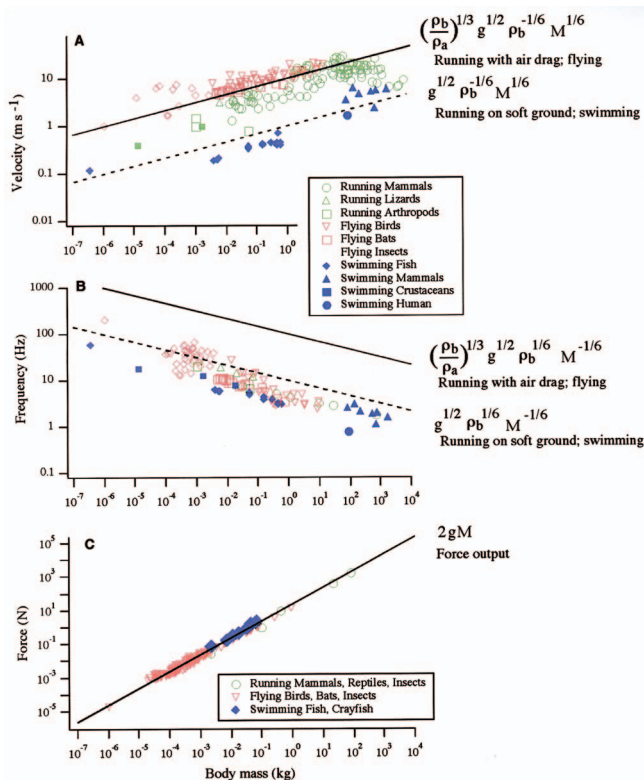


FIG. 18. (Color) Comparison of theoretical predictions with the speeds, stroke frequencies, and force outputs of a wide variety of animals (from Ref. 52 and references therein). The theoretical predictions are based on scale analysis, which neglects factors of order 1 and therefore should be accurate in an order of magnitude sense. Note, however, that in nearly all cases the theory comes closer than order of magnitude agreement with empirical data.

$$St = \frac{t^{-1} L_b}{V_{opt}}, \tag{20}$$

which for optimal flight is a constant:  $St \sim (\rho_a / \rho_b)^{1/3} \sim 10^{-1}$ . This agrees with the large volume of *St* data on animal flight.<sup>70,71</sup>

### D. Running

The speeds and stride frequencies of all runners can be predicted in the same way as flying—as an optimized intermittency in the Earth’s gravitational field.<sup>52</sup> Running is a succession of cycles involving two losses. One loss is the lifting of the body weight to a height comparable with the body length (the limbs), and is calculated as the first term ( $W_1$ ) in Eq. (18). This work is the vertical loss, because when the body lands its gravitational potential energy is destroyed in the legs and the ground. The second is the horizontal loss  $W_2$ : the work performed to overcome friction against the ground, the surrounding air and internal body parts. The horizontal loss depends on the nature of the terrain. In Ref. 52, three models are considered: running on highly deformable ground, hard flat ground, and against air drag. It was found that the horizontal loss model ( $W_2$ ) influences very little the predicted speed and stride frequency.

As in Eq. (18), the vertical and horizontal losses compete, and when they are in balance their sum is minimal. The

optimized intermittency called running is characterized by a speed proportional to  $M^{1/6}$  and a stride frequency proportional to  $M^{-1/6}$ , Figs. 18(A) and 18(B). Noteworthy is the *robustness* of the predictions. The horizontal loss may be dominated by dry friction against a hard surface, permanent deformation (indentation) of a soft surface such as sand, mud and snow, or air drag. All these effects influence the speed and frequency, but they influence them in almost the same way. If air drag is the dominant horizontal loss mechanism, then the speed and frequency deviate by only a factor of order 10 from what they would be for runners with dry friction and ground deformation. The factor 10 is a constant in animal locomotion: 10 is the value of the group  $(\rho_b / \rho_a)^{1/3}$ , where  $\rho_b$  and  $\rho_a$  are the body and air densities. Running dominated by air drag is like flying. Running with dry friction and ground deformation is somewhat slower. The nature of the horizontal loss (habitat and terrain) is random (as in Fig. 7), and this randomness, along with variation in internal friction, is responsible for the scatter that we see in the data for running. That the scatter must be modest is predicted by theory.

### E. Swimming

When one calculates the vertical work spent on lifting the body ( $W_1$ ), one finds that the scale of the vertical muscle force exerted over the stride or stroke cycle is twice the body weight,<sup>52</sup>  $2Mg$ . Figure 18(C) shows that this agrees very well with the force-weight measurements across all body sizes, for all animals that fly, run, and swim. So far we have seen that as an “optimized intermittency” running is similar to flying. But, is it also like swimming?

The seemingly obvious answer is no, because the movement of neutrally buoyant bodies (fish) has nothing to do with gravity. The “intuition” has until recently prevented the emergence of a theory of swimming. The reason why running and swimming are no different than flying (this in spite of the fact that flyers do not touch the ground) is that the ground supports the weight of every body that exists above it. The same ground serves as reference—the much bigger body—against which all moving bodies push horizontally. Without the ground as reference, no locomotion is possible.

How the swimmer balances its vertical and horizontal efforts is shown in Fig. 16(B). To advance horizontally by one body length, the animal body must do work equivalent to lifting a body of water of its own size to a height equal to its body length scale. This body of water must be lifted so that the swimmer may slip under it and advance horizontally. Water is incompressible and the only way for the displaced water to move is up, because the bottom does not move, and because the free surface is deformable. At all but the shallowest depths, this raising of the water surface will be distributed over a large area and therefore imperceptible.

With this, constructal theory of locomotion accounts for swimming. Its predictions of speed and stroke frequency are the same as for running on deformable ground, and the agreement with the numerous data is convincing (Fig. 18).

In summary, a thermodynamics approach can predict complex features of animal design. What constructal theory

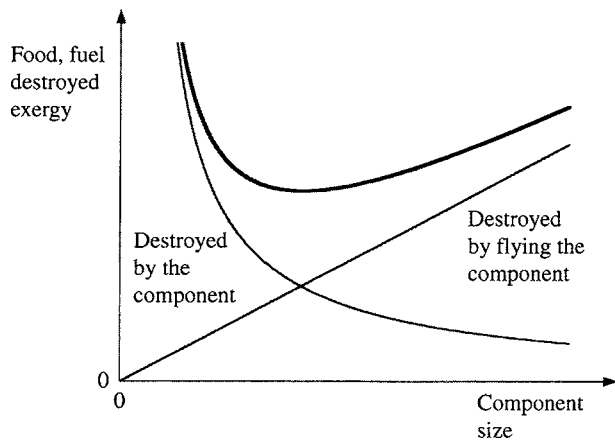


FIG. 19. The origin of the “characteristic size” of the flow component (organ) of a larger flow system (animal) that moves.

shows is that an evolutionary process should consistently and predictably produce runners, swimmers, and fliers with these speeds, stroke/stride frequencies, and force outputs.

## F. Organ size

The pursuit of flow geometry and rhythm also leads to the optimal size that a flow component (an organ) should have in the greater and more complex flow system to which it belongs.<sup>72,73</sup> The total exergy (food and fuel) that an animal or vehicle must consume to travel a specified distance  $L$  is of the order of  $MgL$ . This can be verified by substituting  $V_{\text{opt}}$  of Eq. (19) into Eq. (18).

Consider the need to use a flow component (lung, heart, heat exchanger) on an animal or aircraft that flies. The size of this component is unknown. The component destroys less exergy when it is larger. For example, ducts with larger cross sections require less pumping power (exergy destroyed by fluid friction), and heat exchangers with larger heat transfer surfaces destroy less exergy as well. The first thought then is that bigger is better. This idea is indicated by the downward curve shown in Fig. 19. This thought comes in conflict with the constructal theory of locomotion (Secs. III C–III E), according to which the vehicle or animal must destroy an amount of exergy (fuel and food) that is proportional to the mass of the component. The cost of carrying the component on board is proportional to the mass of the component. This second idea is represented by the rising line in Fig. 19.

Important is the *total* fuel and food consumption, and based on the minimum revealed by Fig. 19 we discover that a flow component has an *optimal size*. The best organ is not the one recommended by the thermodynamics of the organ alone: that would be infinitely large. The best lung for the bird is not the one that has huge air passages. The best lung is compact, svelte,<sup>74</sup> and *imperfect*: it destroys exergy by fluid friction. This gives the impression that “nature makes mistakes,” but to think this way is to miss the big picture. The seemingly imperfect component makes the whole flow system be the best (the least imperfect) that it can be.

## IV. ENGINEERED FLOW CONFIGURATIONS

There is a progression in the flow configurations covered in this review (natural inanimate, animate, and engineered), but it is not an illustration of the practice of copying from nature (Fig. 1). On the contrary, this progression expresses the unity of all flow configurations, i.e., the universality of the phenomenon of generation of flow configuration and the principle that covers it.

In Sec. II we saw how the tree-shaped river basins and the configurations through which the atmospheric and oceanic currents flow (the “climate,” the “turbulence,” etc.) endow the flowing Earth with its constructal quality: paths for maximum flow access, along which the flows dissipate energy against the Earth’s crust, and mix the crust most effectively. In Sec. III we saw that animal movement is another class of flow systems that coexist with and achieve the same things as the inanimate flow systems. Their configuration and rhythm evolve in predictable ways as they shave and reconfigure the Earth’s crust more effectively. In this section we illustrate the practical content of the constructal theory of generation of geometry and rhythm in nature.

### A. Flow spacings

Natural tree-shaped networks are the best flowing routes between one point and an area (or volume) because they bathe the available space with channels of multiple scales, which are allocated optimally to interstitial areas (or volumes). Many scales are organized hierarchically—few are large, many are small—and are distributed nonuniformly. They are positioned in the right places. Optimal bathing, optimal packing, and maximum density of function come from the drawing that consists of multiple scales that are arranged nonuniformly.

The same principle rules the generation of even simpler flow configurations that bathe a finite-size space. A key result of constructal theory is the prediction of optimal spacings<sup>17,75</sup> for the internal flow structure of volumes that must transfer heat and mass to the maximum. This idea is essential in the conceptual design of cooling for electronics of all scales. The idea holds for both forced and natural convections and laminar and turbulent flows. Optimal spacings have been determined for several configurations, depending on the shape of the heat transfer surface that is distributed through the volume: stacks of parallel plates (e.g., Fig. 20), bundles of cylinders in crossflow, arrays of staggered plates, and arrays of pins with impinging flow. This segment of the constructal literature is reviewed in Refs. 6 and 17. In each configuration, the discovery is a single geometric feature: the optimal spacing between solid components. This length scale is distributed uniformly over the available flow space.

For example, in Fig. 20 the flow space is two-dimensional ( $H \times L$ ), the horizontal plates generate heat, and the stack is cooled by forced convection with single-phase fluid of temperature  $T_0$ , which is driven by the fixed pressure difference  $\Delta P$ . The total rate of heat generation installed in the flow space is  $q$ , and the temperature of the plates is  $T_w$ . The global thermal resistance of the package is  $(T_w - T_0)/q$ , and depends on the spacing  $D_0$ , or the number of plates

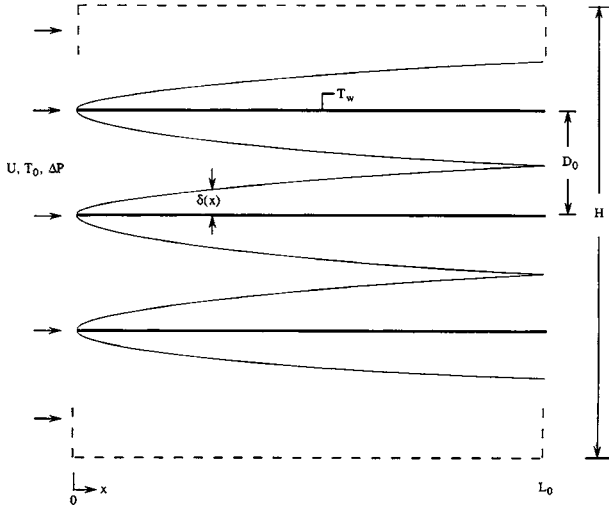


FIG. 20. Optimal construct of parallel plates with laminar forced convection.

( $H/D_0$ ). The global resistance is large in the two extremes, small  $D_0$  and large  $D_0$ . When  $D_0$  is much smaller than the laminar boundary layer thickness sketched in Fig. 20, the coolant cannot flow easily through the package. When  $D_0$  is much larger than the boundary layer thickness, the plates are too few, the thermal contact area between  $T_w$  and coolant is too small, and  $q$  cannot flow out of the plates. These extremes invite a choice between too much fluid-flow resistance and too much heat-transfer resistance. The correct choice is to balance the two negative features so that their global effect is minimum. This balance yields the optimal spacing

$$\frac{D_{0,opt}}{L_0} \cong 2.7Be^{-1/4}, \tag{21}$$

where  $Be$  is the dimensionless group<sup>76,77</sup>  $\Delta PL_0^2/\mu\alpha$ , and  $\mu$  and  $\alpha$  are the fluid viscosity and thermal diffusivity, and the Prandtl number is of order 1 or greater. This optimal distribution of imperfection is achieved when the thermal boundary layers just touch in the exit plane, cf. Fig. 20. In this configuration  $q$  is maximum if the allowable high temperature ( $T_w$ ) is specified. This is the configuration with maximum heat transfer density or maximum compactness (Sec. V).

The optimal spacings for packages with natural convection heat and mass transfer are analogous to those for forced convection.<sup>77</sup> In brief, if the structure of Fig. 20 is rotated by 90° counterclockwise, and if the flow is driven upward by the buoyancy effect, then the role of the overall pressure difference  $\Delta P$  is played by the difference between two hydrostatic pressure heads, one for the fluid column of height  $L_0$  and temperature  $T_0$ , and the other for the  $L_0$  fluid column of temperature  $T_w$ . If the Boussinesq approximation applies, the effective  $\Delta P$  due to buoyancy is<sup>17</sup>  $\Delta P = \rho g \beta \Delta T L_0$ , where  $\Delta T = T_w - T_0$ ,  $\beta$  is the coefficient of volumetric thermal expansion,  $g$  is the gravitational acceleration aligned vertically downward (against  $x$  in Fig. 20), and  $\nu$  is the kinematic viscosity. By substituting the  $\Delta P$  expression into the  $Be$  definition (21) we find that the dimensionless group that replaces

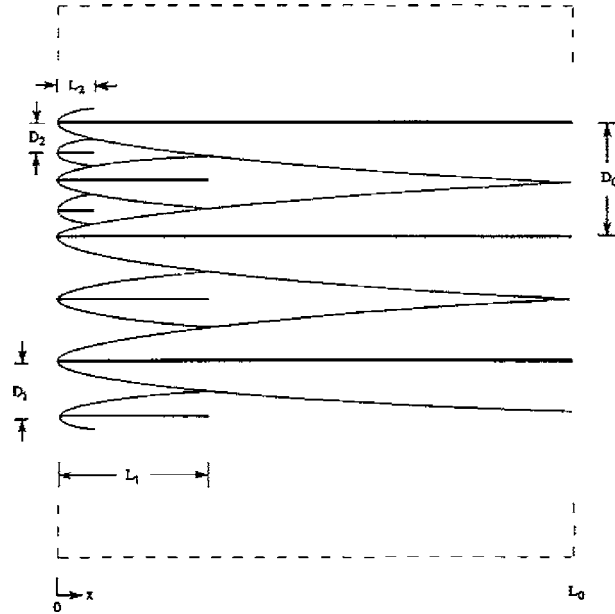


FIG. 21. Multiscale construct of parallel plates (Ref. 78).

$Be$  in natural convection is the Rayleigh number  $Ra = g\beta\Delta TL_0^3/(\alpha\nu)$ . Other than the  $Be \rightarrow Ra$  transformation, all the features that are due to the generation of flow structure for natural convection should mirror, at least qualitatively, the features described for forced convection.

The transport density of the package of Fig. 20 can be increased further by using several length scales and distributing them optimally (nonuniformly). The technique<sup>78</sup> consists of placing more heat transfer in regions of the volume  $HL_0$  where the boundary layers are thinner. Those regions are situated immediately downstream of the entrance plane  $x = 0$ . Regions that do not work in a heat transfer sense must either be put to work or eliminated. In Fig. 20 the wedges of fluid contained between the tips of opposing boundary layers are not involved in transferring heat. They can be involved if heat-generating blades of shorter lengths ( $L_1$ ) are installed on their planes of symmetry. Even shorter plates ( $L_2$ ) are inserted in the smaller mouths formed between plates  $L_1$  and  $L_0$ . This new architecture is shown in Fig. 21. Every length ( $L_1, L_2, \dots$ ) is optimized so that the global heat transfer density is increased. Viewed in profile, the package becomes a comb with teeth of multiple lengths.

This path to the discovery of flow architecture has wider applicability. One example is the configuring of tubes (cylinders) in cross flow, which is the most common flow arrangement used in heat exchanger design. The lesson derived from Fig. 21 is that instead of using a bank of cylinders of one size and one spacing, it is better to use assemblies of cylinders with several diameters.<sup>79</sup> The discovered architecture is illustrated in Fig. 22, where every diameter and spacing is optimized and depends on the overall pressure drop ( $Be$ ). All the spacings decrease as  $Be$  increases, this in agreement with Eq. (21). The most recent work on optimal spacings is presented in Refs. 80–83.

Another example<sup>84</sup> is shown in Fig. 23, where the best way to arrange a number of heat generating components ( $q', D_0$ ) on a wall cooled by laminar forced convection is the

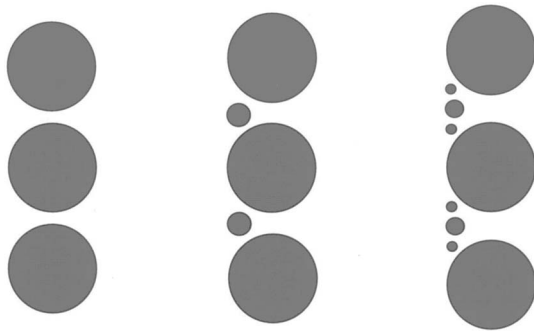


FIG. 22. Multiscale construct of parallel cylinders in cross flow (Ref. 79).

nonuniform, multiscale arrangement. The spacings ( $S_i$ ) must be smaller upstream and larger downstream, and must be zero in a region ( $x_0$ ) near the tip of the boundary layer. Multiscale architectures were also obtained for cooling by natural convection<sup>85</sup> and for walls with heat sources of finite thickness.<sup>86</sup> The architectures of Figs. 21–23 stand in contrast with current designs of cooled electronics, where heat-generating components of equal strength are arranged equidistantly on a substrate.

**B. Trees for heat conduction**

In the cooling of electronics the frontier is being pushed in the direction of smaller dimensions and greater svelteness (Sec. V). There comes a point where miniaturization makes convection cooling impractical, because the fluid channels would take too much space. In this limit, the only way to vehicle the heat out of the package is by conduction. From this argument came the proposal<sup>3</sup> to cool heat-generating volumes by using tree-shaped inserts of high-conductivity blades and fibers.

Trees for conduction cooling are now a growing literature (e.g., Refs. 12 and 87–101). The first conduction trees were generated by using the construction method illustrated here in Figs. 3 and 4. At the elemental level (Fig. 3), the rectangle  $H_0 \times L_0$  is a low-conductivity ( $k_0$ ) material that generates heat volumetrically and uniformly  $q'''$  [W/m<sup>3</sup>]. A blade of constant thickness ( $D_0$ ) and high conductivity ( $k_p$ ) is inserted along the longer of the two axes of the rectangle. The sink ( $T_0$ ) is the left end of the  $k_p$  blades. The hot spots ( $T_{max}$ ) occur in the two right-hand corners of the rectangle. The total heat current is  $q' = q'''H_0L_0$ . The size  $H_0L_0$  is fixed, but the shape ( $H_0/L_0$ ) may vary. The elemental thermal resistance  $(T_{max} - T_0)/q'$  is minimum when

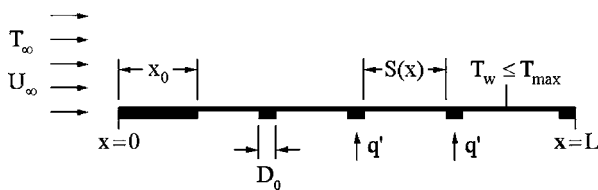


FIG. 23. Multiple length scales on a wall with concentrated heat sources and maximum heat transfer density in laminar forced convection (Ref. 84).

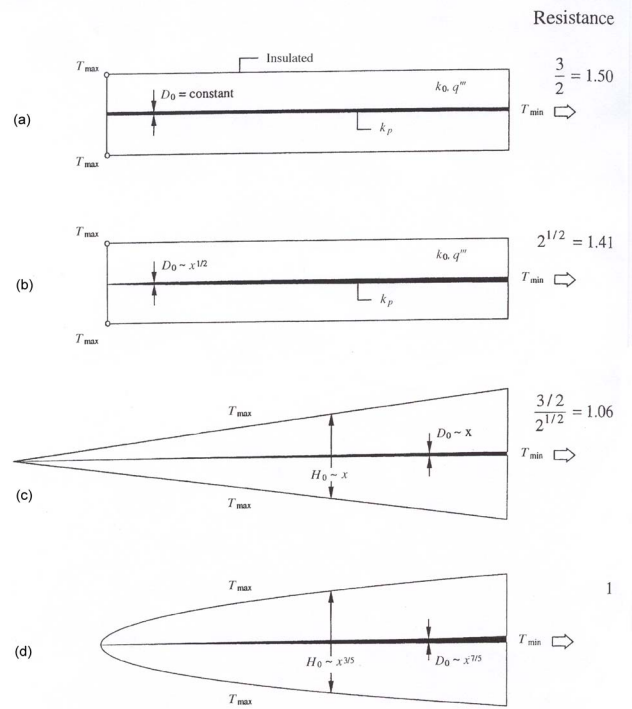


FIG. 24. Elemental conduction volume with progressively greater freedom to morph and progressively higher performance (Ref. 87).

$$H_0/L_0 = (k_0H_0/k_pD_0)^{1/2}, \tag{22}$$

which is a geometric feature equivalent to the one shown in Eq. (3). The generation of the tree continued at large scales, by assembling optimal numbers of smaller constructs into larger constructs (e.g., Fig. 4).

A better tree performance is obtained by endowing the flow configuration with more freedom to morph.<sup>7,8</sup> Ledezma *et al.*<sup>21</sup> used a fully numerical approach in which they replaced the construction sequence of Fig. 4 with numerical simulations of conduction in the composite domain ( $k_0, k_p$ ), with the freedom to vary all the geometric features of the emerging tree structure. First, they abandoned the assumption that the high-conductivity insert is a blade of constant thickness. As shown in the second frame of Fig. 24, the optimal profile of the  $k_p$  insert is such that  $D_0$  increases as  $x^{1/2}$ , where  $x$  is measured away from the tip. Relative to the design of Eq. (22), the decrease in the global thermal resistance of the elemental volume is 6%. Even greater reductions in global thermal resistance result from discarding the assumption that the element is rectangular.<sup>87</sup> The bottom frame of Fig. 24 shows that there is an optimal leaflike elemental shape, as there is an optimal shape for the  $k_p$  fiber. Increasing the freedom to morph the structure leads to higher performance levels and to designs that look *more natural*.

The assumption that the  $k_p$  branches are perpendicular to their stems was also abandoned.<sup>21</sup> For example, in a first construct with  $\tilde{k} = k_p/k_0 = 50$  and  $\phi_1 = V_{p1}/V = 0.1$ , it was found that the optimal angle is such that the branch deviates from the perpendicular by 4°, and that in this refined geometry the global resistance is smaller by 5.8% than before. Angled branches increase the global performance and make the tree architecture look more natural.

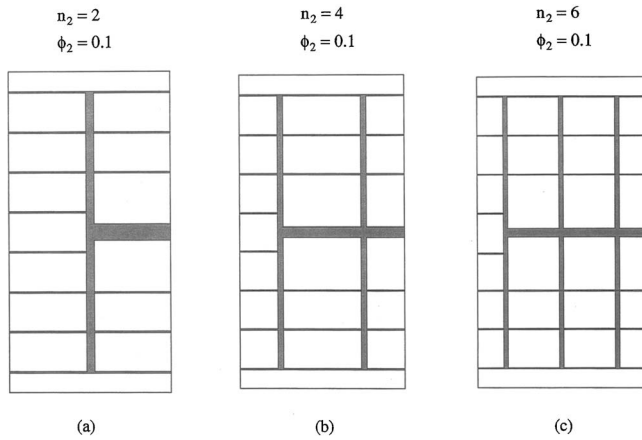


FIG. 25. Second construct optimized numerically, and the effect of changing the number ( $n_2$ ) of high-conductivity inserts of intermediate size ( $D_1$ ) (Ref. 21).

Ledezma *et al.*<sup>21</sup> also abandoned the sequential construction of larger assemblies, and in a composite domain such as Fig. 25 optimized the numbers and positions of every high-conductivity insert. There are three  $k_p$ -blade thicknesses,  $D_0 < D_1 < D_2$ . Because of the increased freedom, the numerical formulation made it possible to omit the thin ( $D_0$ ) branches that would have crowded the stem ( $D_2$ ). Figure 25 was drawn for  $\tilde{k} = k_p/k_0 = 300$ ,  $\phi_2 = V_{p2}/V = 0.1$ ,  $D_1/D_0 = 5$ ,  $D_2/D_1 = 2$ , and eight  $D_0$  blades on one  $D_1$  blade. The purpose of this figure is to illustrate the effect that the number ( $n_2$ ) of  $D_1$  blades has on the global performance. From (a) to (c), the dimensionless global thermal resistance  $\Delta T_2 k_0 / q'' A_2$  takes the values 0.0379, 0.0354, and 0.0374, where  $A_2$  is the total size of the rectangular domain, and  $\Delta T_2$  is the temperature difference between the hot spot (the left corners) and the heat sink (the midpoint of the right side). The competing designs in Fig. 25 show that the best is (b), where the number of  $D_1$  inserts is  $n_2 = 4$ . This result differs from the simplest approach,<sup>3</sup> in which the rule of assembly was pairing (di-

chotomy), i.e.,  $n_2 = 2$ . The result that  $n_2 = 4$  coincides with the optimal construction rule found for river drainage basins in Fig. 4 and Table III.

Figure 25 also shows that the performance of designs (a) and (c) is not too far from that of design (b). This means that tree-shaped flow architectures that have been optimized partially or completely are *robust*. By using the results tabulated in Refs. 1 and 2, one can show that the analytical construction sequence produces a structure with a global resistance ( $\Delta T_2 k_0 / q'' A_2$ ) of the same order of magnitude as in Fig. 25, but larger. This comparison shows the approximate character of the simplest approach, and the merits of increasing the number of degrees of freedom of the structure simulated numerically.

In drawings such as Figs. 4 and 25 we discover tree patterns that maximize flow access. Every detail of the tree geometry is the result of invoking the constructal law. The discovery of the tree as the flow architecture for maximal access between one point and an infinity of points is general—it is not restricted to trees of streets<sup>2</sup> and trees of high-conductivity inserts.<sup>3</sup> The generality of the tree discovery is stressed by Table V, which shows that “how” unites and “what” divides. How the tree is generated (through a balance between high resistivity and low resistivity) is the same in many classes of flow systems, regardless of the diversity of the currents that flow through them. To see the principle that unites is harder than to see the “diversity” of flow systems in nature and engineering.

A related direction of progress on multiscale structures for conduction is the development of optimal rough surfaces for minimal thermal contact resistance.<sup>102–104</sup>

### C. Trees for fluid flow

The tree-flow constructions illustrated in Figs. 3–7 for natural fluid-flow systems are being pursued actively in engineering.<sup>105–118</sup> One objective is to distribute one stream from one inlet to an area or volume. Another objective is to

TABLE V. How the balancing of high resistivity flow with low resistivity flow in a wide diversity of flow systems (courtesy of Stéphen Périm).

Application	What	How	
		Interstices high resistance at the smallest (fixed) scale	Channels low resistance at larger scales
Electronics packages	Heat	Low-conductivity substrate	High-conductivity inserts (blades, needles)
River basins	Water	Darcy flow through porous media	Rivulets and rivers
Lungs	Air	Diffusion in alveoli, tissues	Bronchial passages
Circulatory systems	Blood	Diffusion in capillaries, tissues	Blood vessels, capillaries, arteries, veins
Turbulent flow	Momentum	Laminar, viscous diffusion	Streams, eddies
Urban traffic	People	Walking in urban structure	Street traffic
Economics	Goods	Hand delivery and collection	Freight, rail, truck, air, ship

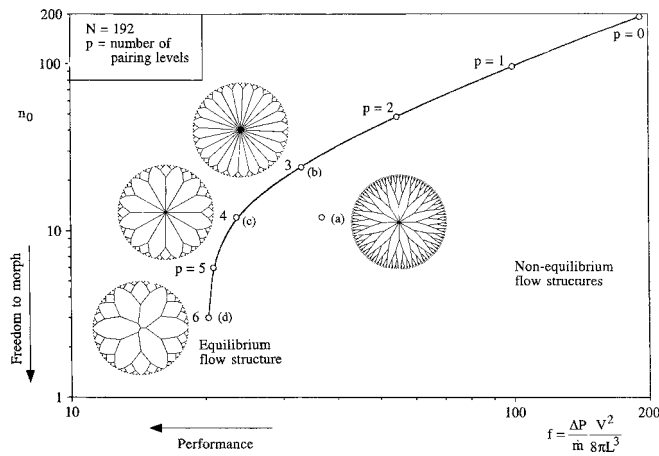


FIG. 26. The performance vs freedom domain of flows that connect the center with  $N$  equidistant points on a circle (Ref. 74).

collect the stream, i.e., to reconstitute it and guide it from the entire area or volume to a single outlet. Both functions are in play in two-stream heat exchangers (see Sec. IV D).

In the work on fluid trees in engineering we see diversity of applications and an effort to understand the properties of tree-shaped flow structures: what features make them better and what strategies should the designer employ to arrive at optimal or near-optimal tree constructs faster and more economically. This fundamental approach is most evident in the development of fluid trees that connect a circle with its center (e.g., Refs. 105 and 115). The center is the source or sink, and the circle is the infinity of points, which in designs for electronics cooling is approximated by a large number of equidistant outlets or inlets (Fig. 26). The flow is in the Poiseuille regime. The ratio of successive tube diameters is chosen based on the Hess-Murray rule,<sup>46</sup> which is an architectural feature in accord with the constructal law. The three-dimensional counterpart of this class of trees is the tree that connects one point with a plane situated at a distance from the point:<sup>106</sup> the resulting tree architecture resembles a showerhead.

Point-circle trees were first drawn by postulating a fixed ratio between successive tube lengths.<sup>115</sup> This layout is shown as inset (a) in Fig. 26. The abscissa indicates the dimensionless global resistance between the center and the rim of the disk,

$$f = \frac{\Delta P}{\dot{m}} \frac{V^2}{8\pi L^3}, \quad (23)$$

where  $\dot{m}$ ,  $\Delta P$ ,  $V$ , and  $L$  are the total mass flow rate, pressure difference, volume of all the tubes, and disk radius. The constraints are the external size ( $L$ ) and the internal size ( $V$ ), and this means that the *svelteness* [ $Sv$ , see Eq. (24)] of all the designs shown in Fig. 26 is the same.

According to the constructal law, the evolution of the point-circle tree configurations in Fig. 26 must be toward the left. This migration is made possible by allowing the tube lengths to vary freely. The configurations shown as (b)–(d) were obtained by optimizing every tube length.<sup>105</sup> The number of pairing or bifurcation levels is  $p$ , and the number of tubes that touch the center is  $n_0$ . Designs (a) and (c) have

$p=4$  as an additional constraint, and show how the freeing of the tube lengths leads to a significant improvement in performance (i.e., a smaller  $f$ ).

Additional improvements are possible if  $p$  is also allowed to vary. In this way the optimal morphing<sup>105</sup> of the tube layout brings the structure to configuration (d), which has  $p=6$ . This was called the *equilibrium flow structure*,<sup>7,8</sup> because in its vicinity of the design space the performance does not change even though it is here that the configuration is the most free to change.

Structures such as (b)–(d) outline a ragged boundary that divides the performance-freedom design space into two domains. To the right are the possible (suboptimal) designs, such as the assumed structure (a). To the left of the (b)–(d) boundary it is impossible to find flow configurations that have the same  $L$ ,  $V$ , and  $Sv$  as configurations (a)–(d).

An important observation is that the best flow structure has finite complexity ( $p=6$ ), not maximum complexity. It would be easy to draw configurations much more complex and crooked than (d), and their performance would be significantly inferior to that of (d). Maximization of performance and morphing freedom in time (the constructal law) does not mean maximization of complexity.

Powerful strategies are emerging for accelerating the search for optimal tree-shaped flow configurations. Effective rules are the Hess-Murray rule for successive duct diameters, dichotomy for Poiseuille flow (Fig. 26), and quadrupling for fully turbulent flow (Fig. 4). Another highly effective shortcut is to select all the duct lengths by minimizing the length of each duct on its allocated flow area.<sup>106</sup> From this follows the shape of every flow area, from the smallest to the largest, and the construction of the entire tree canopy in two or three dimensions. Another strategy is to recognize that in configuration (d) of Fig. 26 the optimized angles of confluence are approximately  $75^\circ$ . This quasi-invariant result was obtained by optimizing Y-shaped constructs of three tubes,<sup>61,105,117</sup> and can be used as a rule for constructing rapidly tree structures that are situated very close to the (b)–(d) boundary in Fig. 26.

The crowding of near-optimal designs near the equilibrium flow structure speaks of the robustness of tree-shaped architectures. Trees that do not look like the best perform practically as well as the best. This is an attractive feature that drives the use of tree flows in engineering. Robustness is increased further by installing loops<sup>107</sup> at the small and intermediate scales of the canopy, so that if one duct is damaged the fluid can flow the other way around the loop and preserve the global performance of the tree flow. Further applications of tree-shaped fluid-flow architectures in civil engineering and urban design are reviewed in Refs. 14 and 119.

## D. Multiobjective flow architectures

Trees for convection are being developed for applications ranging from electronics cooling and photovoltaic cells, to skating rinks, cold storage, and the distribution of hot and chilled waters (e.g., Refs. 120–137). In heat exchanger design the constructal law calls for the maximization of access

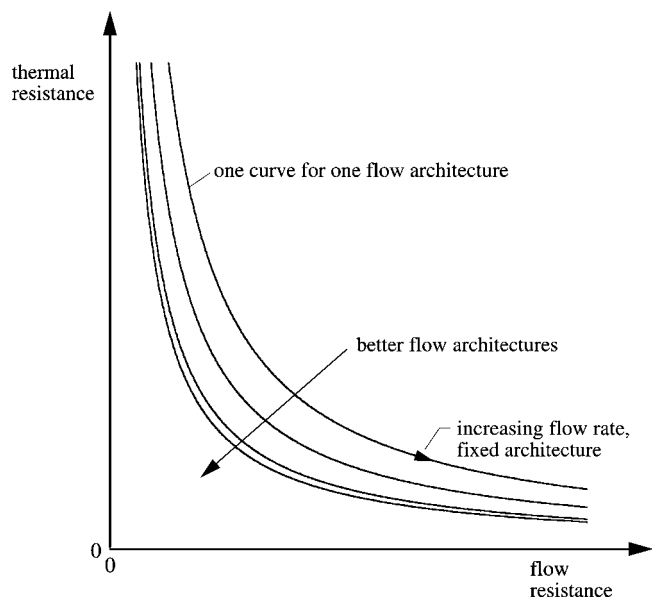


FIG. 27. The time evolution of convective architectures with small thermal resistance and small fluid flow resistance (Ref. 120).

for two flows: (i) heat transfer and (ii) fluid flow. One architecture is better than another if it provides easier access for (i) and (ii) at the same time.

Figure 27 shows schematically how (i) and (ii) are pursued at the same time. A given heat-exchanger architecture is characterized by one curve of thermal resistance ( $R_t$ ) versus fluid-flow resistance or pumping power ( $\dot{W}$ ). Increasing from left to right along the curve is the mass flow rate through the structure. High flow rates mean small  $R_t$  and large  $\dot{W}$ . Attractive are flow architectures with small  $R_t$  and small  $\dot{W}$  at the same time.

The pursuit of small  $R_t$  and small  $\dot{W}$  simultaneously is an example of the more general proposal to morph (to evolve) a structure so that it meets two or more objectives from the start. In constructal theory, this general direction started with the proposal to discover the internal and external configuration of bodies that must serve as flow systems and structural support members at the same time. Examples are cavernous walls that must be mechanically strong and thermally good insulators<sup>138</sup> and beams that must be strong in bending and time resistant to sudden and intense heating (e.g., fire).<sup>139</sup> These applications of constructal theory are important steps in the direction of a scientific approach to the prevention of urban disasters.

An example of the evolution of the flow architecture in the two-objective design space of Fig. 27 is shown in Fig. 28. Here we have three classes of two-stream counterflow heat exchangers, each having the same external size and internal size (total flow volume). The rightmost  $\tilde{R}_t$ - $\tilde{W}$  curves belong to the configuration consisting of two adjacent tubes (the dimensionless thermal resistance  $\tilde{R}_t$  and pumping power  $\tilde{W}$  are defined in Ref. 123). The dashed line corresponds to two disk-shaped sheets of fluid in counterflow. The leftmost curves are for counterflows made of two trees touching like two palms pressed against each other. The curve marked with

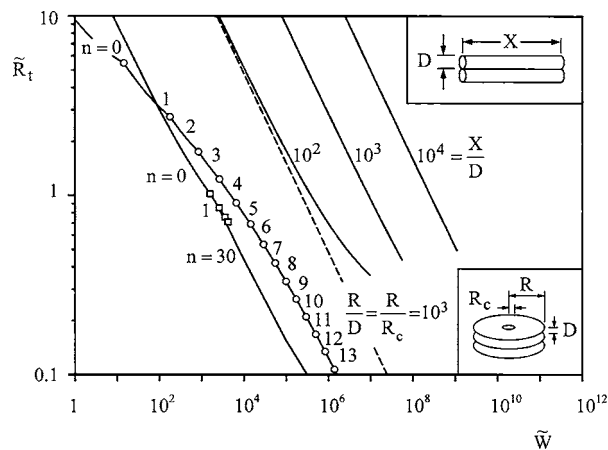


FIG. 28. The evolution of thermo-fluid performance of architectures for two-stream counterflow heat exchangers (Ref. 123): from right to left, two adjacent tubes, two radial flow sheets, and two trees (Fig. 29).

circles corresponds to the configuration shown in Fig. 29, where the two sides of the heat transfer surface are point-circle and circle-point trees of the type optimized as (b)–(d) in Fig. 26. The curve marked with squares is for two trees mounted on a square heat transfer surface. Figure 28 strengthens the evidence in favor of using tree-shaped flow architectures in compact (high density, large  $Sv$ ) transport devices.<sup>123,140–144</sup>

In a 1998 editorial, Bergles<sup>145</sup> foresaw the arrival of a “fourth-generation heat transfer technology, in which heat exchangers will not be eliminated, but they will be greatly reduced in size.” This stepwise change in compactness is exactly what the tree-shaped architectures of constructal theory are now offering. Dendritic heat exchangers have triggered a *vascularization* race not only in heat exchangers but also in electronics cooling, fuel cells architecture conceptualization<sup>140,141,146–149</sup> and fluid distribution and collection in general.

## V. THERMODYNAMICS OF NONEQUILIBRIUM SYSTEMS WITH CONFIGURATION

In constructal theory, body size, architecture, and complexity are results, not assumptions. They are intrinsic parts of the drawing: the optimal configuration to which the flow system tends in time, in accordance with the constructal law. This tendency was recently put on an analytical basis, such that the constructal law becomes a new extension of thermodynamics—the thermodynamics of nonequilibrium (flow) systems with configuration.<sup>7,8,150</sup> This formulation is condensed in Fig. 30.

### A. Properties

A flow system (e.g., a tree) has “properties” that distinguish it from a static (nonflow) system. The properties of a flow system are (1) global external size, e.g., the length scale of the body bathed by the tree flow  $L$ ; (2) global internal size, e.g., the total volume of the ducts  $V$ ; (3) at least one global objective, or performance, e.g., the global flow resistance of the tree  $R$ ; (4) configuration, drawing, architecture; and (5) freedom to morph, i.e., freedom to change the configuration.

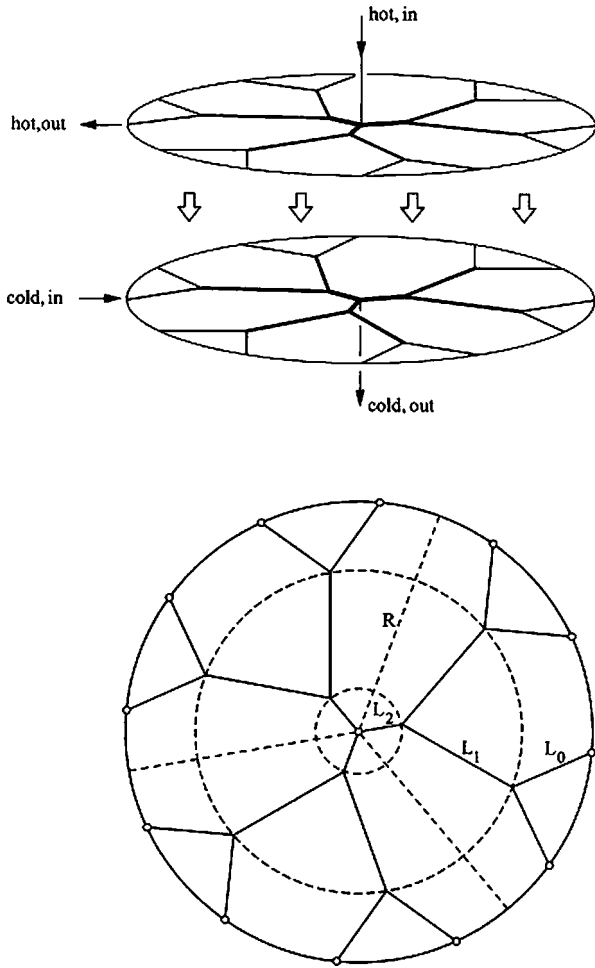


FIG. 29. Counterflow heat exchanger with two point-circle flow trees (Ref. 123) of the types (b)–(d) shown in Fig. 26.

The global external and internal sizes ( $L, V$ ) mean that a flow system has two length scales  $L$  and  $V^{1/3}$ . These form a dimensionless ratio—the *sveltiness*  $S_v$ —which is a new global property of the flow configuration:<sup>74</sup>

$$S_v = \frac{\text{external length scale}}{\text{internal length scale}} = \frac{L}{V^{1/3}}. \tag{24}$$

The flow structures covered by the constructal law populate and move in the  $V=\text{const}$  plane shown in Fig. 30. This plane houses a performance versus freedom diagram: in time, and if the architecture is free to change,  $R$  decreases (i.e., performance increases) at constant  $L$  and  $V$ . The configuration with the smallest  $R$  value represents the equilibrium flow structure. The configurations that preceded it are nonequilibrium flow structures. An illustration of the movement of the flow architecture in time (at constant  $L$  and  $V$ ) was illustrated in Fig. 26. The abscissa parameter  $f$  is the global dimensionless flow resistance for Poiseuille flow between the center of a circle and  $N=192$  points distributed equidistantly on the circle. The parameter  $f$  corresponds to the performance parameter  $R$  in Fig. 30. At equilibrium (d) the flow configuration achieves the most that its freedom to morph has to offer.

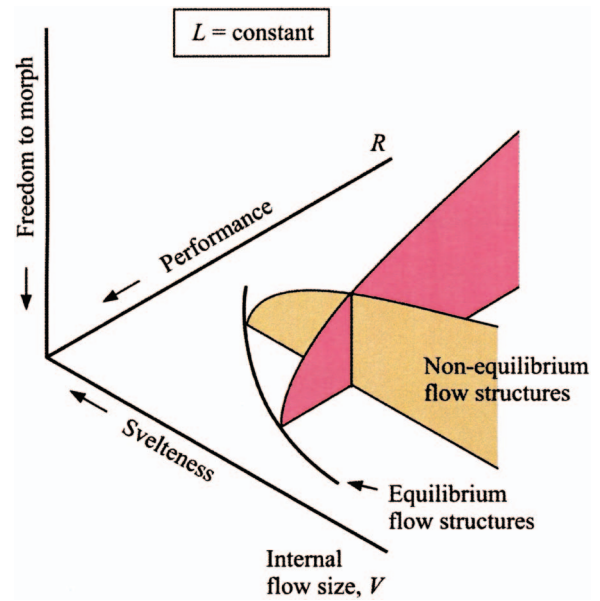


FIG. 30. (Color) Performance vs freedom to change configuration, at fixed global external size (Refs. 7 and 8).

### B. Survival by increasing performance

The evolution of configurations in the constant- $V$  cut (also at constant  $L$ , Fig. 30) represents survival through increasing performance—survival of the fittest. This is the physics principle that now underpins the Darwinian argument, the physics law that rules not only the animate flow systems but also the natural inanimate flow systems and all the man and machine species. The constructal law defines the meaning of “the survivor” or of the equivalent concept of “the more fit.” The constructal-law idea that freedom to morph is good for performance (Fig. 30) also accounts for the Darwinian argument that the survivor is the one most capable to adapt.

In the bottom plane of Fig. 30 the locus of equilibrium structures is a curve with negative slope,  $(\partial R / \partial V)_L < 0$ , because of flow physics: the resistance decreases when the size of the internal space inhabited by the flow increases. This slope means that the nonequilibrium flow structures occupy the body suggested by the three-dimensional surface sketched in Fig. 30. The time evolution of nonequilibrium flow structures toward the bottom edge of the surface (the equilibrium structures) is the action of the constructal law.

### C. Survival by increasing sveltiness (compactness)

The same time arrow can be described alternatively with reference to the constant- $R$  cut through the three-dimensional space of Fig. 30. Flow architectures with the same global performance ( $R$ ) and global size ( $L$ ) evolve toward compactness and sveltiness—smaller volumes dedicated to internal ducts, i.e., larger volumes reserved for the working “tissue” (the interstices). Paraphrasing the original statement of the constructal law, we may describe the evolution at constants  $L$  and  $R$  as follows:

For a system with fixed global size and global performance to persist in time (to live), it must evolve in such a

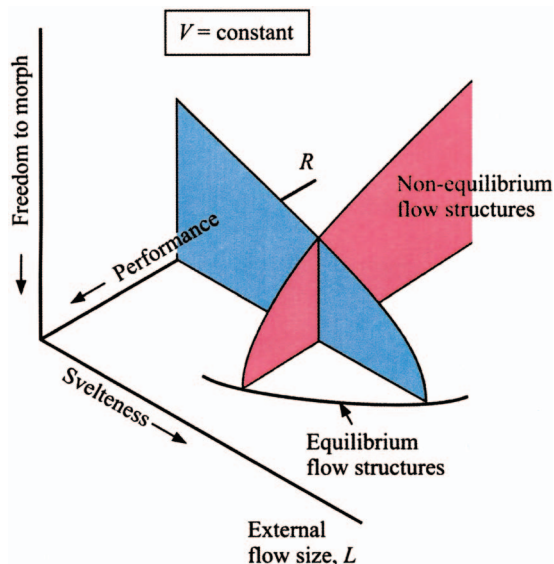


FIG. 31. (Color) Performance vs freedom to change configuration, at fixed global internal size (Refs. 7 and 8).

way that its flow structure occupies a smaller fraction of the available space. This is survival based on the maximization of the use of the available space. Survival by increasing sveltiness (compactness) is equivalent to survival by increasing performance: both statements are the constructal law.

#### D. Survival by increasing flow territory

A third equivalent statement of the constructal law becomes evident if we recast the constant- $L$  design world of Fig. 30 in the constant- $V$  design space of Fig. 31. In this new figure, the constant- $L$  cut is the same performance versus freedom diagram as in Fig. 30, and the constructal law means survival by increasing performance. The contribution of Fig. 31 is the shape and orientation of the hypersurface of nonequilibrium flow structures: the slope of the curve in the bottom plane  $(\partial R/\partial L)_V$  is positive because of flow physics, i.e., because the flow resistance increases when the distance traveled by the stream increases.

The world of possible designs can be viewed in the constant- $R$  cut made in Fig. 31, to see that flow structures of a certain performance level ( $R$ ) and internal flow volume ( $V$ ) morph into new flow structures that cover progressively larger territories. Again, flow configurations evolve toward greater sveltiness  $S_v$ . The constructal law statement becomes:

In order for a flow system with fixed global resistance ( $R$ ) and internal size ( $V$ ) to persist in time, the flow architecture must evolve in such a way that it covers a progressively larger territory. There is a limit to the spreading of a flow structure, and it is set by global properties such as performance (technology) and internal flow volumes  $R$  and  $V$ .

River deltas in the desert, animal species on the plain, and the Roman empire spread to their limits. Such is the constructal law of survival by spreading, by increasing territory for flow and movement. Now we know why this should be so.<sup>74</sup>

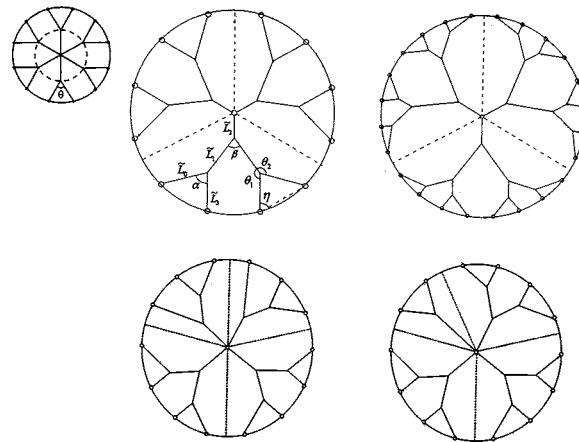


FIG. 32. More freedom “to morph” leads to higher performance and asymmetry in the circle-point tree networks of Fig. 26 (after Ref. 109).

#### E. Freedom to morph is good for performance

In many of the examples given in this review we illustrated the morphing and generating of progressively better tree-shaped flow networks. We did this by focusing on trees that connect a circle with its center. The summary given in Fig. 26 shows that when there are 192 equidistant points on the circle the equilibrium flow architecture has a certain (optimized, finite) degree of complexity, which is represented by six levels of bifurcation or pairing.

More recently, we discovered<sup>109</sup> that the circle-point tree architectures can be morphed and improved further, so that their points migrate even farther to the left on the performance versus freedom domain of Fig. 26. The true equilibrium flow architecture lies slightly to the left of the point (d). The path to this higher level of performance is made possible by increasing the freedom of the morphing architecture. How this is done is explained in Fig. 32. The upper-left frame illustrates the type of circle-point trees that has been studied by a significant body of literature until now. It is based on the reasonable assumption that at each level of pairing or bifurcation the mother tube splits into two daughter tubes that have the same length. This assumption is so “reasonable” and so popular that no one questioned it. In truth, however, any simplifying assumption that the designer makes is a straight jacket that curtails the freedom of the morphing architecture.

The other frames of Fig. 32 show what happens to the tree architecture when the assumption of daughter tubes of equal length is not made. We have discovered in this way the emergence of several types of asymmetry in equilibrium tree architectures: different tube lengths at the same level of branching, different mass flow rates at junctions, and different main branches.<sup>109</sup> The emergence of *asymmetry* in the best tree networks (made-made or natural) is the fingerprint of the constructal law in action.

#### VI. CONCLUSION

The real world (nature, physics) has architecture, organization, and pattern. The tissues of energy flow systems such as the fabric of society and all the tissues of biology, are optimized architectures. Not just “any” architectures, as in

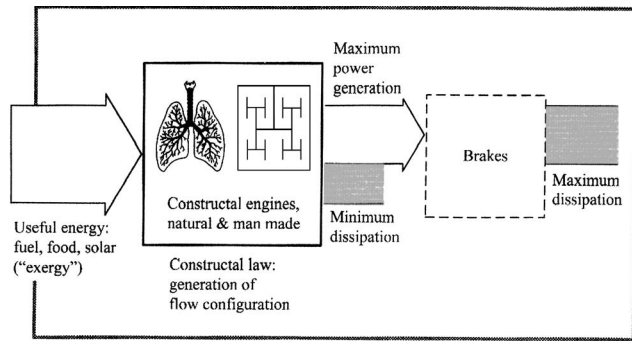


FIG. 33. Every nonequilibrium (flow) component of the earth functions as an engine that drives a brake (Refs. 13 and 31). The constructal law governs “how” the system functions: by generating a flow architecture that distributes imperfections optimally to fill the flow space (e.g., Table V). As a consequence, the “engine” part evolves in time toward generating maximum power (or minimum dissipation), and the “brake” part does the rest: maximum dissipation. Evolution means that each flow system assures its persistence (survival) in time by freely morphing into easier and easier flow structures under global finiteness constraints. The arrows proceed from left to right because this is the general drawing for a flow (nonequilibrium) system, in steady or unsteady state. When equilibrium is reached, all the flows cease, and the arrows disappear.

the black boxes of classical thermodynamics, but the optimal, or the near-optimal architectures (Sec. V). The climbing to this high podium of performance is the transdisciplinary effort—the balance between seemingly unrelated flows, territories, and disciplines.

No flow system is an island. No river exists without its wet plain. No city thrives without its farmland and open spaces. Everything that flowed and lived to this day to “survive” is in an optimal balance with the flows that surround it and sustain it. This balancing act—the optimal distribution of imperfection—generates the very design of the process, power plant, city, geography, and economics.

In this article we reviewed on the basis of constructal theory the physics phenomena of generation of flow configuration in nature, which are now covered by the thermodynamics of nonequilibrium (flow) systems with configuration.<sup>7,8</sup> The new and most basic development is this: there are two time arrows in thermodynamics, not one. The old is the time arrow of the second law of thermodynamics, the arrow of irreversibility: everything flows from high to low. The new is the time arrow of the constructal law, the arrow of how every flowing thing acquires architecture. The “how” is condensed in the constructal law: existing configurations assure their survival by morphing in time toward easier flowing configurations. The constructal time arrow unites physics with biology and engineering.

We see this union in Fig. 33, which expresses the vision proposed in Fig. 3.16 of Ref. 1 and earlier. The Earth with its solar heat input, heat rejection, and wheels of atmospheric and oceanic circulation, is a heat engine without shaft: its maximized (but not ideal) mechanical power output cannot be delivered to an extraterrestrial system. Instead, the Earth engine is destined to dissipate through air and water friction and other irreversibilities (e.g., heat leaks along finite  $\Delta T$ 's) all the mechanical power that it produces. It does so by “spinning in its brake” the fastest that it can (hence the winds and the ocean currents, which proceed along easiest routes).

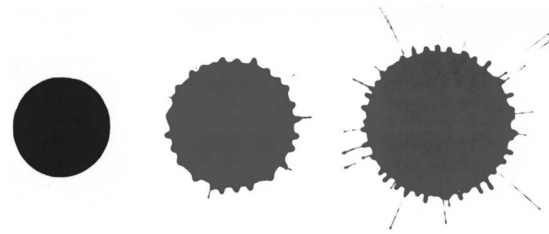


FIG. 34. Splat vs splash configuration, after a liquid droplet impacts a wall. If the droplet is small and slow enough, it comes to rest viscously as a disk. If the droplet is large and fast enough, it splashes into needles that grow radially until they are arrested by viscous effects.

Because the flowing Earth is a constructal heat engine, its flow configuration has evolved in such a way that it is the least imperfect that it can be. It produces a maximum power, which it then dissipates at maximum rate. As shown in Sec. II H, maximum dissipation has been invoked *ad hoc* in geophysics: all such discussion refers to what goes on only in the brake.

The “engines” of engineering and biology (power plants and animal motors) have shafts, rods, legs, and wings that deliver the mechanical power to external entities that use the power (e.g., vehicles and animal bodies needing propulsion). Because the engines of engineering and biology are constructal, they morph in time toward flow configurations that make them the least imperfect that they can be. Therefore they evolve toward producing maximum mechanical power (under finiteness constraints), which, for them, means a time evolution toward minimum dissipation (minimum entropy generation rate).

On the outside of an engineering or biology engine, all the mechanical power that the engine delivers is destroyed through friction and other irreversibility mechanisms (e.g., transportation and manufacturing for man, animal locomotion and body heat loss to ambient). The engine and its immediate environment (the brake), as one thermodynamic system, are analogous to the whole Earth (Fig. 33).

The field of constructal theory and design is expanding very rapidly. During the peer-review phase of this article, new papers related to constructal theory were written on the scaling laws of river basins,<sup>151</sup> dendritic agglomeration of dust particles,<sup>152</sup> heat loss from mantle convection,<sup>153</sup> dendritic versus spherical morphology of stony corals,<sup>154</sup> dendritic solid-gas chemical reactors,<sup>155</sup> scaling laws of animal design,<sup>156</sup> pulsating and dendritic heat transfer through biological tissues,<sup>157,158</sup> dendritic and morphing architectures for heat exchanger design,<sup>159–165</sup> prediction of onset of turbulence in boundary layer flow,<sup>166</sup> and the vascularization of the next generation of smart material structures endowed with distributed *self-healing* and *self-cooling* properties.<sup>167–171</sup>

A related development is the theoretical prediction of electrodiffusion through porous materials.<sup>172</sup> When a species concentration difference and a current are imposed at  $t=0$  across a diffusing medium, the species is transported by two mechanisms: classical diffusion and “convection” driven by the imposed current. At short times, diffusion is more effective and dominates. At longer times, convection is the domi-

nating mechanism. The action of the constructal law is evident because at any given moment the flow mechanism that is selected is such that the flow access of the species is maximized. The competition between the two mechanisms is qualitatively similar to what we presented in the lower part of Fig. 9. This development has significant implications in the mathematical description of electrodiffusion and the maximization of performance of species decontamination processes.

Another development is the prediction of configuration generation during liquid droplet impact on a wall<sup>173</sup> (Fig. 34). If the droplet is small and slow enough, the “splat” comes to rest viscously, as a disk. If the droplet is large and fast enough, it “splashes” by developing needles that grow radially until they are arrested by viscous effects. The transition between splat and splash behavior is crucial in modern technologies (spray coating, painting, ink jet printing) and forensic medicine. The constructal law predicts that the dimensionless group ( $G$ ) that governs the splat-splash selection is the ratio of two lengths: the final radius of the disk (splat) that dies viscously, divided by the radius of the still inviscid ring that just wrinkles. Splats form when  $G \leq O(1)$ , and splashes are favored when  $G \geq O(1)$ . The  $G$  number is the same as  $(We Re^{1/2})^{1/5}$ , where  $We$  and  $Re$  are the Weber and Reynolds numbers of the droplet before impact. Experimental measurements reported in the literature confirm the main features of the constructal development of splat vs. splash flow architecture.<sup>173</sup>

In summary, the body of work reviewed for the first time in this article introduces a paradigm that is universally applicable in natural sciences (physics and biology), engineering, and social sciences.

<sup>1</sup>A. Bejan, *Advanced Engineering Thermodynamics*, 2nd ed. (Wiley, New York, 1997).

<sup>2</sup>A. Bejan, *J. Adv. Transp.* **30**, 85 (1996).

<sup>3</sup>A. Bejan, *Int. J. Heat Mass Transfer* **40**, 799 (1997).

<sup>4</sup>A. Bejan, *Int. J. Heat Mass Transfer* **40**, 2097 (1997).

<sup>5</sup>A. Bejan, *Int. J. Therm. Sci.* **36**, 592 (1997).

<sup>6</sup>A. Bejan, *Shape and Structure, from Engineering to Nature* (Cambridge University Press, Cambridge, UK, 2000).

<sup>7</sup>A. Bejan and S. Lorente, *Int. J. Heat Mass Transfer* **47**, 3203 (2004).

<sup>8</sup>A. Bejan and S. Lorente, *La Loi Constructale* (L'Harmattan, Paris, 2005).

<sup>9</sup>H. Poirier, *Science & Vie* 1034, 44 (2003).

<sup>10</sup>R. N. Rosa, A. H. Reis, and A. F. Miguel, *Bejan's Constructal Theory of Shape and Structure* (Évora Geophysics Center, University of Évora, Portugal, 2004).

<sup>11</sup>N. Torre, *La Macchina del Tempo* 5, 36 (2004).

<sup>12</sup>J. Lewins, *Int. J. Heat Mass Transfer* **46**, 1541 (2003).

<sup>13</sup>A. Bejan, *Advanced Engineering Thermodynamics*, 3rd ed. (Wiley, Hoboken, NJ, 2006).

<sup>14</sup>A. Bejan, I. Dincer, S. Lorente, A. F. Miguel, and A. H. Reis, *Porous and Complex Flow Structures in Modern Technologies* (Springer, New York, 2004).

<sup>15</sup>C. R. Carrigan and J. C. Eichelberger, *Nature* (London) **343**, 248 (1990).

<sup>16</sup>C. R. Carrigan, in *Magmatic Systems*, edited by M. P. Ryan (Academic, New York, 1994), pp. 319–353.

<sup>17</sup>A. Bejan, *Convection Heat Transfer*, 3rd ed. (Wiley, Hoboken, NJ, 2004).

<sup>18</sup>J. G. Cervantes, F. J. Solorio, and F. Méndez, *J. Fluids Struct.* **17**, 1203 (2003).

<sup>19</sup>L. B. Leopold, M. G. Wolman, and J. P. Miller, *Fluvial Processes in Geomorphology* (Freeman, San Francisco, 1964).

<sup>20</sup>A. E. Scheidegger, *Theoretical Geomorphology*, 2nd ed. (Springer-Verlag, Berlin, 1970).

<sup>21</sup>G. A. Ledezma, A. Bejan, and M. R. Errera, *J. Appl. Phys.* **82**, 89 (1997).

<sup>22</sup>M. R. Errera and A. Bejan, *Fractals* **6**, 245 (1998).

<sup>23</sup>A. Bejan, S. Lorente, A. F. Miguel, and A. H. Reis, *Advanced Engineering Thermodynamics* (Ref. 13), Sec. 13.5.

<sup>24</sup>A. Klarbring, J. Petersson, B. Torstenfelt, and M. Karlsson, *Comput. Methods Appl. Mech. Eng.* **192**, 3909 (2003).

<sup>25</sup>A. R. Kacimov, *Proc. R. Soc. London, Ser. A* **462**, 1409 (2006).

<sup>26</sup>A. Bejan, Y. Ikegami, and G. A. Ledezma, *Int. J. Heat Mass Transfer* **41**, 1945 (1998).

<sup>27</sup>P. Bartelt and O. Buser, *J. Glaciol. Geocryol.* **50**, 342 (2004).

<sup>28</sup>R. A. Nelson, Jr. and A. Bejan, *J. Heat Transfer* **120**, 357 (1998).

<sup>29</sup>W. V. R. Malkus, *Proc. R. Soc. London, Ser. A* **225**, 196 (1954).

<sup>30</sup>A. Bejan and A. H. Reis, *Int. J. Energy Res.* **29**, 303 (2005).

<sup>31</sup>A. H. Reis and A. Bejan, *Int. J. Heat Mass Transfer* **49**, 1857 (2006).

<sup>32</sup>E. N. Lorenz, *Tellus* **7**, 157 (1955).

<sup>33</sup>G. W. Paltridge, *Q. J. R. Meteorol. Soc.* **101**, 475 (1975).

<sup>34</sup>L. L. Schulman, *J. Atmos. Sci.* **34**, 559 (1977).

<sup>35</sup>G. W. Paltridge, *Q. J. R. Meteorol. Soc.* **104**, 927 (1978).

<sup>36</sup>G. R. North, *Rev. Geophys. Space Phys.* **19**, 91 (1981).

<sup>37</sup>C. A. Lin, *Geophys. Res. Lett.* **9**, 716 (1982).

<sup>38</sup>R. D. Lorenz, J. I. Lunine, C. P. McKay, and P. G. Withers, *Geophys. Res. Lett.* **25**, 415 (2001).

<sup>39</sup>J. M. Gordon and Y. Zarmi, *Am. J. Phys.* **57**, 995 (1989).

<sup>40</sup>A. De Vos and G. Flater, *Am. J. Phys.* **59**, 751 (1991).

<sup>41</sup>A. De Vos, *Endoreversible Thermodynamics of Solar Energy Conversion* (Oxford University Press, Oxford, UK, 1992).

<sup>42</sup>A. De Vos and P. Van der Wel, *Theor. Appl. Climatol.* **46**, 193 (1993).

<sup>43</sup>A. H. Reis, A. F. Miguel, and M. Aydin, *Med. Phys.* **31**, 1135 (2004).

<sup>44</sup>K. Schmidt-Nielsen, *Scaling: Why is Animal Size so Important?* (Cambridge University Press, Cambridge, UK, 1984).

<sup>45</sup>*Principles of Animal Design*, edited by E. R. Weibel, C. R. Taylor, and L. Bolis (Cambridge University Press, Cambridge, UK, 1998).

<sup>46</sup>E. R. Weibel, *Symmorphosis* (Harvard University Press, Cambridge, MA, 2000).

<sup>47</sup>B. K. Ahlborn, *Zoological Physics* (Springer, Berlin, 2004).

<sup>48</sup>J. A. Adam, *Mathematics in Nature* (Princeton University Press, Princeton, NJ, 2003).

<sup>49</sup>*Scaling Functions to Body Size: Theories and Facts*, edited by H. Hoppeler and E. R. Weibel, *J. Exp. Biol.* **208**, 9 (2005).

<sup>50</sup>A. Bejan, *J. Exp. Biol.* **208**, 1677 (2005).

<sup>51</sup>A. Bejan, *Int. J. Heat Mass Transfer* **44**, 699 (2001).

<sup>52</sup>A. Bejan and J. H. Marden, *J. Exp. Biol.* **209**, 238 (2006).

<sup>53</sup>G. B. West, J. H. Brown, and B. J. Enquist, *Science* **276**, 122 (1997).

<sup>54</sup>F. Seebacher, *J. Theor. Biol.* **203**, 97 (2000).

<sup>55</sup>P. W. Hochachka, C.-A. Darveau, R. D. Andrews, and R. K. Suarez, *Comp. Biochem. Physiol. A* **134**, 675 (2003).

<sup>56</sup>A. Majumdar, A. M. Alencar, S. V. Buldyrev, Z. Hantos, E. H. Stanley, and B. Suki, *Phys. Rev. E* **67**, 031912 (2003).

<sup>57</sup>V. J. Menon and D. C. Agrawal, *Am. J. Phys.* **71**, 474 (2003).

<sup>58</sup>M. L. Roderick and B. Barnes, *Funct. Ecol.* **18**, 197 (2004).

<sup>59</sup>B. Barnes and M. L. Roderick, *Theor. Popul. Biol.* **66**, 113 (2004).

<sup>60</sup>J. G. Chaui-Berlink, C. A. Navas, L. H. A. Monteiro, and J. E. P. W. Bicudo, *J. Exp. Biol.* **208**, 1709 (2005).

<sup>61</sup>A. Bejan, L. A. O. Rocha, and S. Lorente, *Int. J. Therm. Sci.* **39**, 949 (2000).

<sup>62</sup>A. Bejan, *Int. J. Heat Mass Transfer* **22**, 219 (1979).

<sup>63</sup>S. Weinbaum and L. J. Jiji, *J. Biomech. Eng.* **107**, 131 (1985).

<sup>64</sup>A. Bejan, A. M. Morega, G. B. West, and J. H. Brown, *Phys. Today* **58**(7), 20 (2005).

<sup>65</sup>A. Bejan, *J. Heat Transfer* **112**, 662 (1990).

<sup>66</sup>A. Bejan, *Int. J. Heat Mass Transfer* **33**, 206 (1990).

<sup>67</sup>A. Bejan, *Heat Transfer* (Wiley, New York, 1993).

<sup>68</sup>H. Tennekes, *The Simple Science of Flight* (MIT, Cambridge, MA, 1996).

<sup>69</sup>E. Frey, H. Tischlinger, M.-C. Buchy, and D. M. Martill, in *Evolution and Palaeobiology of Pterosaurs*, edited by E. Buffetaut and J.-M. Mazin (Geological Society, Special Publications, London, 2003), pp. 233–266.

<sup>70</sup>N. C. Heglund, C. R. Taylor, and T. A. McMahon, *Science* **186**, 1112 (1974).

<sup>71</sup>G. K. Taylor, R. L. Nudds, and A. L. R. Thomas, *Nature* (London) **425**, 707 (2003).

<sup>72</sup>A. Bejan and S. Lorente, International Mechanical Engineering Congress and Exposition, New Orleans, 17–22 November 2002, ASME Paper IM-ECE 2002-33158.

<sup>73</sup>J. C. Ordóñez and A. Bejan, *Int. J. Therm. Sci.* **42**, 335 (2003).

- <sup>74</sup>S. Lorente and A. Bejan, *Int. J. Therm. Sci.* **44**, 1123 (2005).
- <sup>75</sup>A. Bejan and E. Sciuabba, *Int. J. Heat Mass Transfer* **35**, 3259 (1992).
- <sup>76</sup>S. Bhattacharjee and W. L. Grosshandler, *ASME HTD* **96**, 711 (1988).
- <sup>77</sup>S. Petrescu, *Int. J. Heat Mass Transfer* **37**, 1283 (1994).
- <sup>78</sup>A. Bejan and Y. Fautrelle, *Acta Mech.* **163**, 39 (2003).
- <sup>79</sup>T. Bello-Ochende and A. Bejan, *Int. J. Heat Mass Transfer* **48**, 1373 (2005).
- <sup>80</sup>T. Bello-Ochende and A. Bejan, *Int. J. Heat Mass Transfer* **46**, 1693 (2003).
- <sup>81</sup>L. Gosselin, *Int. Commun. Heat Mass Transfer* **33**, 30 (2006).
- <sup>82</sup>H.-Y. Li, S.-M. Chao, and G.-L. Tsai, *Int. J. Heat Mass Transfer* **48**, 5386 (2005).
- <sup>83</sup>R. S. Matos, T. A. Laursen, J. V. C. Vargas, and A. Bejan, *Int. J. Therm. Sci.* **43**, 477 (2004).
- <sup>84</sup>A. K. da Silva, S. Lorente, and A. Bejan, *Int. J. Heat Mass Transfer* **47**, 2139 (2004).
- <sup>85</sup>A. K. da Silva, S. Lorente, and A. Bejan, *Int. J. Heat Mass Transfer* **47**, 203 (2004).
- <sup>86</sup>A. K. da Silva, S. Lorente, and A. Bejan, *Int. J. Heat Mass Transfer* **48**, 2662 (2005).
- <sup>87</sup>M. Neagu and A. Bejan, *J. Appl. Phys.* **86**, 1136 (1999).
- <sup>88</sup>N. Dan and A. Bejan, *J. Appl. Phys.* **84**, 3042 (1998).
- <sup>89</sup>A. D. Kraus, *International Mechanical Engineering Congress and Exposition*, Washington, DC, 21 November 2003, ASME Paper IMECE2003-42381.
- <sup>90</sup>W. Nakayama, *Int. J. Heat Mass Transfer* **46**, 3397 (2003).
- <sup>91</sup>Z.-Z. Xia, X.-G. Cheng, Z.-X. Li, and Z.-Y. Guo, *J. Enhanced Heat Transfer* **11**, 119 (2004).
- <sup>92</sup>F. Bobaru and S. Rachakonda, *Int. J. Heat Mass Transfer* **47**, 4953 (2004).
- <sup>93</sup>F. Bobaru and S. Rachakonda, *Int. J. Numer. Methods Eng.* **60**, 1215 (2004).
- <sup>94</sup>G. Miranda, H. P. L. Luna, G. R. Mateus, and R. P. M. Ferreira, *Comput. Oper. Res.* **32**, 2937 (2005).
- <sup>95</sup>A. R. Kacimov, *Heat Mass Transfer* (in press, 2006).
- <sup>96</sup>A. K. da Silva, C. Vasile, and A. Bejan, *Int. J. Heat Mass Transfer* **47**, 4257 (2004).
- <sup>97</sup>M. A. Almogbel, *Int. J. Therm. Sci.* **44**, 342 (2005).
- <sup>98</sup>C. Biserni, L. A. O. Rocha, and A. Bejan, *Int. J. Heat Mass Transfer* **47**, 2577 (2004).
- <sup>99</sup>L. A. O. Rocha, E. Lorenzini, and C. Biserni, *Int. Commun. Heat Mass Transfer* **32**, 1281 (2005).
- <sup>100</sup>D. Voytovych, S. Artemenko, and V. Mazur, *Fourth International Conference Computational Heat and Mass Transfer*, Proceedings of the Fourth ICCHMT, Paris-Cachan, 17–20 May, 2005.
- <sup>101</sup>G. F. Jones and S. Ghassemi, *ASME Heat Transfer/Fluids Engineering Summer Conference*, Charlotte, NC, 11–15 July 2004.
- <sup>102</sup>M. Neagu and A. Bejan, *J. Heat Transfer* **123**, 1184 (2001).
- <sup>103</sup>J. V. C. Vargas and A. Bejan, *J. Heat Transfer* **124**, 1218 (2002).
- <sup>104</sup>M. G. Blyth and C. Pozrikidis, *Int. J. Heat Mass Transfer* **46**, 1329 (2003).
- <sup>105</sup>W. Wechsato, S. Lorente, and A. Bejan, *Int. J. Heat Mass Transfer* **45**, 4911 (2002).
- <sup>106</sup>S. Lorente, W. Wechsato, and A. Bejan, *Int. J. Heat Mass Transfer* **45**, 3299 (2002).
- <sup>107</sup>W. Wechsato, S. Lorente, and A. Bejan, *Int. J. Heat Mass Transfer* **48**, 573 (2005).
- <sup>108</sup>W. Wechsato, S. Lorente, and A. Bejan, *Numer. Heat Transfer, Part A* **48**, 731 (2005).
- <sup>109</sup>L. Gosselin and A. Bejan, *J. Appl. Phys.* **98**, 104903 (2005).
- <sup>110</sup>H. Brod, *J. Non-Newtonian Fluid Mech.* **111**, 107 (2003).
- <sup>111</sup>D. Tondeur and L. Luo, *Chem. Eng. Sci.* **59**, 1799 (2004).
- <sup>112</sup>W. Wechsato, S. Lorente, and A. Bejan, *Int. J. Heat Mass Transfer* **44**, 3111 (2001).
- <sup>113</sup>W. Wechsato, S. Lorente, and A. Bejan, *Int. J. Heat Mass Transfer* **45**, 723 (2002).
- <sup>114</sup>L. Gosselin, *Int. J. Heat Mass Transfer* **48**, 2159 (2005).
- <sup>115</sup>D. V. Pence, *Microscale Thermophys. Eng.* **6**, 319 (2002).
- <sup>116</sup>A. Y. Alharbi, D. V. Pence, and R. N. Cullion, *J. Fluids Eng.* **125**, 1051 (2003).
- <sup>117</sup>L. Gosselin and A. Bejan, *Int. J. Therm. Sci.* **44**, 53 (2005).
- <sup>118</sup>J.-M. Commenge, L. Falk, J.-P. Corriou, and M. Matlosz, *C. R. Phys.* **5**, 597 (2004).
- <sup>119</sup>A. Bejan and S. Lorente, *J. Non-Equilib. Thermodyn.* **26**, 305 (2001).
- <sup>120</sup>W. Wechsato, S. Lorente, and A. Bejan, *Int. J. Heat Mass Transfer* **46**, 4381 (2003).
- <sup>121</sup>Y. Chen and P. Cheng, *Int. J. Heat Mass Transfer* **45**, 2643 (2002).
- <sup>122</sup>Y. Chen and P. Cheng, *Int. Commun. Heat Mass Transfer* **32**, 931 (2005).
- <sup>123</sup>A. K. da Silva, S. Lorente, and A. Bejan, *J. Appl. Phys.* **96**, 1709 (2004).
- <sup>124</sup>S. Gheorghiu and M.-O. Coppens, *AIChE J.* **50**, 812 (2004).
- <sup>125</sup>Y. Azoumah, N. Mazet, and P. Neveu, *Int. J. Heat Mass Transfer* **47**, 2961 (2004).
- <sup>126</sup>Y. S. Muzychka, *Int. J. Heat Mass Transfer* **48**, 3119 (2005).
- <sup>127</sup>A. Bejan and M. R. Errera, *Int. J. Heat Mass Transfer* **43**, 3105 (2000).
- <sup>128</sup>C. Zamfirescu and A. Bejan, *Int. J. Heat Mass Transfer* **46**, 2785 (2003).
- <sup>129</sup>F. Lundell, B. Thonon, and J. A. Gruss, *Second Conference on Microchannels and Minichannels*, Rochester, NY, 2004.
- <sup>130</sup>M. Lallemand, F. Ayela, M. Favre-Marinet, A. Gruss, D. Maillet, P. Marty, H. Peerhossaini, and L. Tadrist, *Congrès Français de Thermique*, SFT 2005, Reims, 30 May–2 June 2005.
- <sup>131</sup>C. Zamfirescu and A. Bejan, *Int. J. Refrig.* **28**, 231 (2005).
- <sup>132</sup>A. Bejan, *Int. J. Heat Mass Transfer* **45**, 4607 (2002).
- <sup>133</sup>A. Bejan and M. R. Errera, *Fractals* **5**, 685 (1997).
- <sup>134</sup>N. Kockman, T. Kiefer, M. Engler, and P. Woias, *ECI International Conference Heat Transfer and Fluid Flow in Microscale*, Castelvecchio Pascoli, Italy, 25–30 September 2005.
- <sup>135</sup>X.-Q. Wang, A. S. Mujumdar, and C. Yap, *Int. J. Therm. Sci.* (2006).
- <sup>136</sup>A. M. Morega and A. Bejan, *Int. J. Green Energy* **2**, 233 (2005).
- <sup>137</sup>A. Bhakta and S. Bandyopadhyay, *Int. J. Thermodyn.* **8**, 175 (2005).
- <sup>138</sup>S. Lorente and A. Bejan, *Int. J. Heat Mass Transfer* **45**, 3313 (2002).
- <sup>139</sup>L. Gosselin, S. Lorente, and A. Bejan, *Int. J. Heat Mass Transfer* **47**, 3477 (2004).
- <sup>140</sup>S. M. Senn and D. Poulikakos, *J. Power Sources* **130**, 178 (2004).
- <sup>141</sup>S. M. Senn and D. Poulikakos, *J. Appl. Phys.* **96**, 842 (2004).
- <sup>142</sup>A. K. Pramanick and P. K. Das, *Int. J. Heat Mass Transfer* **48**, 1974 (2005).
- <sup>143</sup>A. K. Pramanick and P. K. Das, *Int. J. Heat Mass Transfer* **48**, 1851 (2005).
- <sup>144</sup>A. K. Pramanick and P. K. Das, *Int. J. Heat Mass Transfer* **49**, 1420 (2006).
- <sup>145</sup>A. E. Bergles, *HVAC&R Res.* **4**, 117 (1998).
- <sup>146</sup>J. V. C. Vargas and A. Bejan, *Int. J. Energy Res.* **28**, 319 (2004).
- <sup>147</sup>J. V. C. Vargas, J. Ordóñez, and A. Bejan, *Int. J. Heat Mass Transfer* **47**, 4177 (2004).
- <sup>148</sup>J. V. C. Vargas, J. C. Ordóñez, and A. Bejan, *Int. J. Heat Mass Transfer* **48**, 4410 (2005).
- <sup>149</sup>L. Gosselin and A. Bejan, *J. Appl. Phys.* **96**, 5852 (2004).
- <sup>150</sup>A. Bejan and S. Lorente, *International Mechanical Engineering Congress and Exposition*, Washington, DC, 16–21 November 2003, ASME Paper IMECE 2003-41167.
- <sup>151</sup>A. H. Reis, *Geomorphology* **77**, in press (2006).
- <sup>152</sup>A. H. Reis, A. F. Miguel, and A. Bejan, *J. Phys. D* **39**, 2311 (2006).
- <sup>153</sup>A. Lenardic, L.-N. Moresi, A. M. Jelinek, and M. Manga, *Earth Planet. Sci. Lett.* **234**, 317 (2005).
- <sup>154</sup>A. F. Miguel, *J. Theor. Biol.* (in press).
- <sup>155</sup>Y. Azoumah, P. Neveu, and N. Mazet, *Int. J. Therm. Sci.* **45**, 716 (2006).
- <sup>156</sup>B. Andresen, J. S. Shiner, and D. E. Uehlinger, *Proc. Natl. Acad. Sci. U.S.A.* **99**, 5822 (2002).
- <sup>157</sup>R. Magin, S. Boregowda, and C. Deodhar, *Int. J. Design & Nature* **1**, 18 (2007).
- <sup>158</sup>W. Dai, A. Bejan, X. Tang, L. Zhang, and R. Nassar, *J. Appl. Phys.* **99**, 104702 (2006).
- <sup>159</sup>R. Hilbert, G. Janiga, R. Baron, and D. Thévenin, *Int. J. Heat Mass Transfer* **49**, 2567 (2006).
- <sup>160</sup>T. H. Ko, *Int. J. Therm. Sci.* **45**, 729 (2006).
- <sup>161</sup>B. Yu and B. Li, *Phys. Rev. E* **73**, 066302 (2006).
- <sup>162</sup>G. Lorenzini and L. A. O. Rocha, *Int. J. Heat Mass Transfer* (in press).
- <sup>163</sup>Y. S. Muzychka, *Int. J. Therm. Sci.* **45**, in press (2006).
- <sup>164</sup>T. Dias, Jr. and L. F. Milanez, *Int. J. Heat Mass Transfer* **49**, 2090 (2006).
- <sup>165</sup>A. Horvat and B. Mavko, *Numer. Heat Transfer, Part A* **49**, 699 (2006).
- <sup>166</sup>E. J. Walsh, D. H. Hernon, D. M. McEligot, M. R. D. Davies, and A. Bejan, *Proceedings GT2006, Turbo Expo 2006: Power for Land, Sea and*

Air, Barcelona, 8–11 May 2006.

<sup>167</sup> S. R. White, N. R. Sottos, J. Moore, P. Geubelle, M. Kessler, E. Brown, S. Suresh, and S. Viswanathan, *Nature (London)* **409**, 794 (2001).

<sup>168</sup> D. Therriault, S. R. White, and J. A. Lewis, *Nat. Mater.* **2**, 265 (2003).

<sup>169</sup> K.-M. Wang, S. Lorente, and A. Bejan, *J. Phys. D* **39**, 3086 (2006).

<sup>170</sup> A. Bejan, S. Lorente, and K.-M. Wang, *J. Appl. Phys.* **100**, in press (2006).

<sup>171</sup> S. Kim, S. Lorente, and A. Bejan, *J. Appl. Phys.* (in press).

<sup>172</sup> P. Bégué and S. Lorente, *J. Porous Media* **9**(7) (2006).

<sup>173</sup> A. Bejan and D. Gobin, *Int. J. Heat Mass Transfer* **49**, 2412 (2006).